Nanoscale ZnO doping in prosthetic polymers mitigate wear particle-induced inflammation and osteolysis through inhibiting macrophage secretory autophagy

Zhuocheng Lyu [a,1], Xiangchao Meng [b,1], Fei Hu [a,1], Yuezhou Wu [a], Yurun Ding [a], Teng Long [a], Xinhua Qu [a], You Wang [a,*]

[a] Department of Bone and Joint Surgery, Department of Orthopedics, Renji Hospital, School of Medicine, Shanghai Jiaotong University, Shanghai, China
[b] Department of Orthopedics, Minhang Hospital, Fudan University, Shanghai, China

ARTICLE INFO

ABSTRACT

Wear particles produced by joint replacements induce inflammatory responses that lead to periprosthetic osteolysis and aseptic loosening. However, the precise mechanisms driving wear particle-induced osteolysis are not fully understood. Recent evidence suggests that autophagy, a cellular degradation process, plays a significant role in this pathology. This study aimed to clarify the role of autophagy in mediating inflammation and osteolysis triggered by wear particles and to evaluate the therapeutic potential of zinc oxide nanoparticles (ZnO NPs).

We incorporated ZnO into the prosthetic material itself, ensuring that the wear particles inherently carried ZnO, providing a targeted and sustained intervention. Our findings reveal that polymer wear particles induce excessive autophagic activity, which is closely associated with increased inflammation and osteolysis. We identified secretory autophagy as a key mechanism for IL-1β secretion, exacerbating osteolysis. Both *in vitro* and *in vivo* experiments demonstrated that ZnO-doped particles significantly inhibit autophagic overactivation, thereby reducing inflammation and osteolysis.

In summary, this study establishes secretory autophagy as a critical mechanism in wear particle-induced osteolysis and highlights the potential of ZnO-doped prosthetic polymers for targeted, sustained mitigation of periprosthetic osteolysis.

1. Introduction

Periprosthetic osteolysis, a major cause of aseptic loosening in joint replacements, is primarily driven by the inflammatory response to wear particles generated from implant material[1–5]. The potential application of new polymers in artificial joints further complicates the mechanism of wear particle disease[6–8]. Polyetheretherketone (PEEK) has emerged as an alternative to conventional metallic material due to its excellent mechanical properties, biocompatibility, and radiolucency [9–12]. Our previous clinical trial of PEEK-on-HXLPE knee arthroplasty demonstrated a satisfactory prognosis after two years, but concerns about long-term wear particle-induced osteolysis remain [13]. With repetitive movements under loading, PEEK prostheses might inevitably generate wear debris in the joint microenvironment that triggers an innate immune response, leading to local inflammation and bone loss.

Macrophages are key mediators in this process, responding to wear particles by secreting pro-inflammatory cytokines, including tumor necrosis factor-α (TNF-α), interleukin (IL)-1, IL-6, and macrophage colony-stimulating factor (M-CSF) that promote osteoclastogenesis and bone resorption[14–16]. Multiple researches have indicated that macrophages also possess the differentiation potential of fully functional osteoclasts in response to inflammation triggered by wear particles [17, 18].

Recent studies have also implicated autophagy, a cellular degradation and recycling mechanism, in the pathology of periprosthetic osteolysis [19]. Overactivated autophagy in response to wear particles may exacerbate inflammation and osteolysis, while inhibiting autophagy has been shown to reduce these effects[20–22]. In addition to the classic role of autophagy in protein degradation, there is a growing body of evidence suggesting that the autophagy machinery promotes the

unconventional secretion of leaderless proteins via a process called secretory autophagy [23,24]. During the disturbed homeostasis of the immune system induced by inflammation and infection, the autophagy machinery can redirect part of its cargo into exosomes for secretion, with the goal of actively providing information to neighboring cells and alerting immunity to emerging threats. Several inflammatory proteins such as IL-1β, IL-6, IL-18, and high mobility group box 1 (HMGB1) have been identified as targets of secretory autophagy. Interestingly, all of these inflammatory proteins are known to be involved in the periprosthetic tissues and stimulate osteoclastogenesis [25,26]. Thus, autophagy and its crucial role in the secretion of inflammatory cytokines could be a critical process in wear particle-induced osteolysis and aseptic loosening.

Given the lack of approved therapies for periprosthetic osteolysis, developing biomaterials that minimize wear debris is crucial. Developing novel wear-resistant biomaterials that minimize wear debris formation may be a potential effective approach. Applying zinc oxide nanoparticles (ZnO NPs) in the composite material of prosthetic polymer

to decrease wear debris shed light on the potential biological strategies to prevent aseptic loosening [27,28]. In our previous research, ZnO NPs (50 nm, 5 μg/mL) attenuated polymer wear particle-induced inflammation via regulation of the MEK-ERK-COX-2 axis and reduced bone tissue damage caused by wear debris-induced osteolysis [29]. Several studies have indicated that ZnO nanoparticles can affect macrophages' phagocytosis and autophagy while inhibiting macrophages' activation stimulated with lipopolysaccharide (LPS) [30].

In this study, we demonstrated that autophagy was stimulated in macrophages in the presence of wear debris, and secretory autophagy was involved in the pathogenesis of wear particle-induced periprosthetic osteolysis. Moreover, we modified the composition of PEEK-on-HXLPE prostheses by doping ZnO NPs into the polymer matrix. The wear debris generated by the ZnO-modified composite materials (PEEK-ZnO and PE-ZnO) interfered with the autophagy process and attenuated the inflammation and osteolysis *in vitro* and *in vivo*. Scheme 1 illustrates the general mechanism of secretory autophagy in polymer wear debris-induced periprosthetic osteolysis and the protective effect of nanoscale
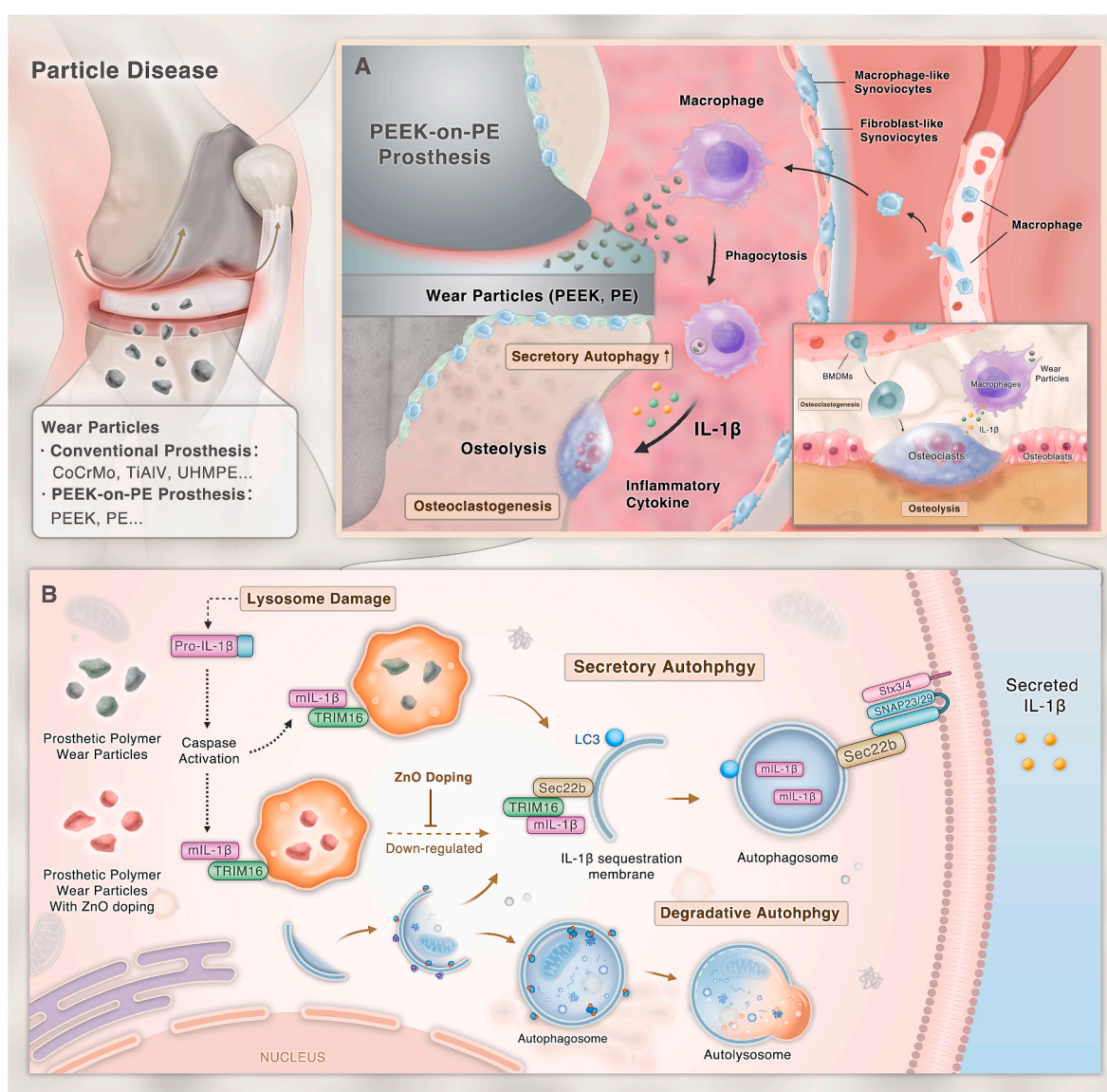
Scheme 1. Graphical abstract of the current study. (A)Macrophages at the implant site and those migrating from distant locations phagocytose wear particles (such as PEEK and PE), leading to the secretion of inflammatory cytokines such as IL-1β. These cytokines then promote osteoclast activation and bone resorption, contributing to periprosthetic osteolysis. (B) In macrophages, wear particles cause lysosomal damage, leading to the activation of caspase, which converts pro-IL-1β into mature IL-1β (mIL-1β). This mIL-1β is then secreted extracellularly through secretory autophagy, mediated by TRIM16 and Sec22b. ZnO-containing wear particles inhibit this secretory autophagy pathway, thereby reducing the secretion of IL-1β.

ZnO doping to attenuate inflammation and osteolysis. Overall, our findings suggest that ZnO-modified materials reduce autophagy-related inflammation and osteolysis, highlighting secretory autophagy as a promising therapeutic target for mitigating periprosthetic osteolysis.

2. Materials and methods

2.1. Material preparation and characterization

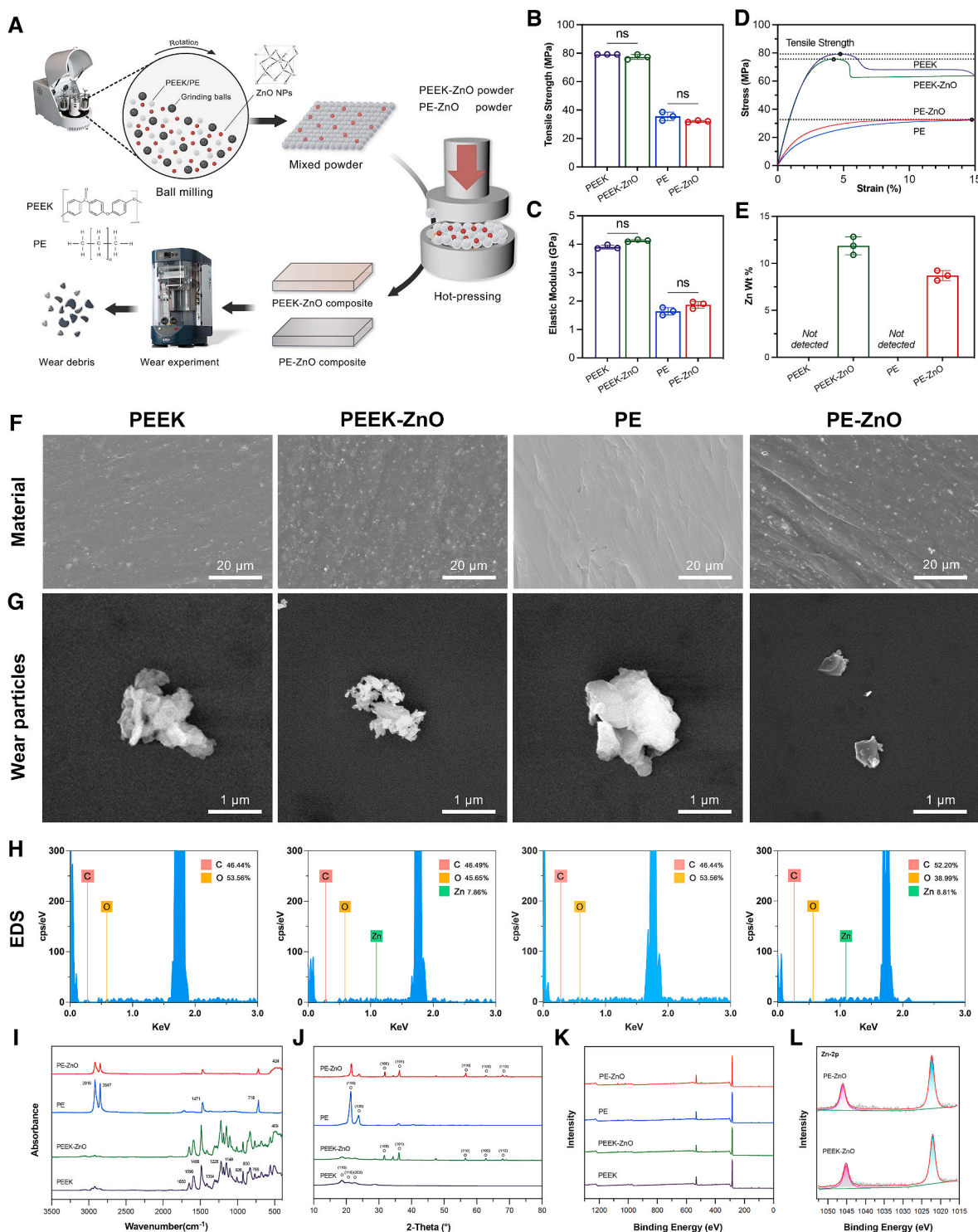**Materials:** PEEK (VICTREX Technology Centre, UK.); XLPE

Fig. 1. Fabrication and characterization of the wear debris. (A) Schematic illustration of materials preparation. The average tensile strength (B) for the PEEK, PEEK-ZnO, PE, and PE-ZnO groups was 79.20 MPa, 77.37 MPa, 35.63 MPa, and 32.11 MPa, respectively, while the average elastic modulus (C) was 3.901 GPa, 4.127 GPa, 1.642 GPa, and 1.868 GPa, respectively. (D) The stress-strain curves of different groups. (E) The average weight content distribution of the Zinc element in the PEEK-ZnO and PE-ZnO groups was 11.87 % and 8.705 %, respectively. Each bar represents the average of three independent samples. (F) SEM images of the fabricated materials. (G) SEM images of the wear particles. (H) EDS mapping and spectrum of different elements in different wear particles. FT-IR (I) and XRD (J) patterns of the wear particles. Broad XPS spectrum of the fully scanned region (K) and the (L) Zn 2p region of the wear particles.

(Borealis, Austria); ZnO nanoparticles (MedChemExpress, USA)

Preparation of wear particles: Fig. 1A illustrates the detailed fabrication process. First, pure PEEK and HXLPE materials were fabricated using a compression molding process. To prepare the PEEK/ZnO composite material. PEEK powder and ZnO nanoparticles (10 wt%) were dried in a vacuum oven at 120 °C for 12 h. Next, they were ball-milled mixed in a planetary ball mill (Emax, Germany) at 25 °C and 400 rpm for 2 h. Finally, the PEEK/ZnO composite material was fabricated by compression molding. Similarly, the PE/ZnO composite material was fabricated using the same procedure. The fabricated materials were then applied to the wear experiment using UMT-3 (Bruker Corporation, USA). After the wear experiment, the samples were cleaned with acetone to remove and collect the generated wear particles. Wear particles from different material samples were donated as PEEK, PE, PEEK-ZnO, and PE-ZnO groups.

Characterization and mechanical property test: The morphology and element composition of the composite materials and wear particles were examined using a field emission scanning electron microscopy (FE-SEM, TESCAN MIRA LMS, Czech Republic) equipped with energy-dispersive X-ray spectrometry (EDS), X-ray photoelectron spectroscopy (XPS, Thermo Scientific K-Alpha, USA), FT-IR (Thermo Scientific Nicolet iS5, USA) as well as X-ray diffraction (XRD, Rigaku Ultima IV, Japan). To assess the mechanical properties of the pure PEEK, PE, and ZnO-doped composite materials, we analyzed the stress-stain curve of all samples using a universal testing machine (Instron 5567, USA). The values of elastic modulus and tensile strength were obtained according to the results of the stress-strain curve. Particle size analysis is achieved using a Malvern laser particle size analyzer.

2.2. In vitro analysis of wear particle-induced cellular responses

Cells: RAW264.7 cells were obtained from ATCC (USA). The detailed procedure of the bone marrow-derived macrophages (BMDMs) extraction is illustrated in Supporting Information.

Reagents: Dulbecco's modified Eagle's medium (DMEM) and fetal bovine serum (FBS) were purchased from Sigma-Aldrich (USA). Cytokines, including RANKL, LPS, and M-CSF, were purchased from MedChemExpress (USA). Chloroquine, Torin1, phalloidin-FITC, and Tartrate-Resistant Acid Phosphatase (TRAP) stain kit was purchased from Sigma-Aldrich (USA). ELISA kits (IL-1β, TNF-α) were purchased from Elab Sciences (China). Reverse transcription (RT) reagents and SYBR Green were purchased from TaKaRa (Japan). Cell counting kit 8 (CCK-8) was purchased from Dojindo (Japan).

Antibodies: NFATc1 (Proteintech 66,963–1), CTSK (Santa Cruz sc-48353), TRAP (Abcam ab52750); LC3B (Sigma L7543); LC3B (MBL PM036); IL-1β (Abcam ab9722); TNF-α (Abcam, ab183218); Sec22b (Abcam ab181076); β-actin (Abcam ab8226); TRIM16 (Santa Cruz sc-79770); ATG16L1 (MBL PM040); WIPI2 (Abcam ab105459); FIP200 (Abcam ab313620); Goat Anti-Rabbit IgG Cy3 (Abcam ab6939); Goat Anti-Mouse IgG FITC (Abcam ab6785);

Cell viability assay: Cell viability assay was performed by CCK-8 assay. RAW264.7 cells were cultured in 96-well microplates overnight (100 μL, 5000 cells per well). Then, the culture media were replaced with 100 μL of fresh media containing PBS or wear particles with gradient concentrations. After 12 h or 24 h of treatment, the cells were rinsed with PBS thrice, and the CCK-8 working solution was added. After 1.5 h of co-incubation, the absorbance at a wavelength of 450 nm was determined with a microplate reader (BioTek, USA).

Real-time PCR (RT-PCR): RNA was extracted by TRIzol reagent, followed by reverse transcription reactions employing the PrimeScript RT kit (Takara, China). The housekeeping gene β-actin expression levels were utilized to standardize the expression levels of the genes of interest. The primers for real-time PCR are available in Table S1 of the Supporting Information.

ELISA assay: According to the manufacturer's recommendations (Elab Sciences, China), ELISA was utilized to detect IL-1β and TNF-α

levels in cell culture supernatants and tissue homogenate.

Western Blot Analysis: Briefly, after treatment, total protein was extracted using RIPA lysis buffer supplemented with 0.1 % phenyl-methylsulfonyl fluoride (PMSF). The lysates were then centrifuged at 15,000×g for 15 min at 4 °C, and the supernatants were carefully collected. Protein concentration was determined using a BCA protein assay kit following the manufacturer's instructions. Subsequently, proteins were denatured by heating at 100 °C for 10 min. Equal amounts of protein from each sample were loaded onto 10 % sodium dodecyl sulfate-polyacrylamide gels for separation by electrophoresis (SDS-PAGE). After electrophoresis, the proteins were transferred onto poly-vinylidene difluoride (PVDF) membranes. The membranes were then blocked with 5 % skimmed milk in TBST (Tris-buffered saline with 0.1 % Tween 20) for 1 h to prevent nonspecific binding. Following the blocking step, the membranes were incubated overnight at 4 °C with primary antibodies diluted in 5 % (w/v) skimmed milk in TBST. After washing, the membranes were incubated with HRP-conjugated secondary antibodies for 1.5 h at room temperature. Protein bands were visualized using an enhanced chemiluminescence (ECL) reagent and detected with a Bio-Rad imaging system. The primary antibodies used in this study were as follows: NFATc1 (66,963–1, Proteintech, 1:3000), CTSK (sc-48353, Santa Cruz, 1:500), TRAP (ab52750, Abcam, 1:5000), β-actin (ab8226, Abcam, 1:1000), SQSTM1 (H00008878-M01, Abnova, 1:1000), and LC3 (L7543, Sigma-Aldrich, 1:1000).

Transwell culture and osteoclast differentiation assay: To evaluate the interaction between wear particle-challenged macrophages and BMDMs, we designed a double-chamber transwell (0.4 μm) system (Fig. 4A). F-actin and TRAP staining were performed after 7 days of co-culturing. Bone slice absorption assay was performed after 10 days of co-culturing. The detailed culture condition and procedure of osteoclast differentiation and assessment are illustrated in Supplementary Material.

Co-localization analysis: For the co-localization of LC3/IL-1β, LC3/Sec22b, and LC3/TRIM16, FIJI (version 2.14.0) software was used to analyze the CLSM images of the wear particle-challenged macrophages. Co-localization was measured by Pearson coefficient using the Coloc2 plugin of the software. For the 3D co-localization, the multichannel image series were reconstructed and analyzed using IMARIS software (Bitplane, Switzerland). IMARIS Coloc function was employed for visualization and quantification of the co-localization level.

Autophagy flux assay: To evaluate the dynamic process of autophagy in the normal synovial cells, an autophagy flux assay by treatment with chloroquine and Torin1 was performed following the protocol [31]. Autophagy was examined by quantification of LC3B-II and p62 levels in response to Torin1 (50 nM) and Torin1 (50 nM) + CQ (50 μM) treatment.

Immunofluorescence assays (IFAs): RAW264.7 cells were co-cultured in wear particle groups with PEEK, PE, PEEK-ZnO, and PE-ZnO wear particles (50 μg/μL) for 12 h, respectively. The immunofluorescence procedure involves the collection, fixation, and blocking of cells. To evaluate the level of inflammation response, the cells were stained with antibodies targeting IL-1β and TNF-α. To evaluate the level of autophagy, the cells were stained with antibodies targeting LC3, WIPI2, FIP200, and ATG16L. Subsequently, the cells were subjected to incubation with the corresponding secondary antibodies and counter-stained with DAPI for 0.5 h, after which they were observed under CLSM.

2.3. In vivo evaluation of wear particle-induced inflammation and osteolysis

Animals: Male C57BL/6 mice (4–6 weeks) were purchased from Shanghai Jiesijie Laboratory Animal Co., Ltd. (China). Male adult Labrador dogs were purchased from Shanghai Jiagan Biotechnology Co., Ltd. (China). All animal experiments performed in this research were approved by the Animal Ethical Committee of the Renji Hospital,

Shanghai Jiaotong University, School of Medicine (Shanghai, China).

Total hip arthroplasty model and proteomic study of labrador dogs using PEEK-HXLPE prostheses: 6 healthy adult Labrador dogs aged 2–5 years were selected. Animals underwent a pre-study veterinary examination, including blood tests and orthopedic evaluation, to ensure they were free from musculoskeletal abnormalities and systemic illnesses. After general anesthesia, we performed a lateral approach to the hip, excised the femoral head and neck, and prepared the acetabulum and femoral canal according to the dimensions of the PEEK-HXLPE prostheses. Insert the prosthetic components, ensuring stability and optimal positioning. Finally, surgical sites are closed in layers using absorbable sutures for musculature and skin. At the end of the 18-month study period, after euthanasia, synovial fluid samples were carefully collected from the implanted joint under sterile conditions. The fluid was extracted using a sterile syringe with a fine-gauge needle and prepared for proteomic analysis using Data-Independent Acquisition (DIA).

Intra-articular injection of wear particles in mice: All the animal procedures and experiments were approved by the Animal Ethical Committee of the Renji Hospital, Shanghai Jiaotong University, School of Medicine (Shanghai, China). We obtained 50 male C57BL/6 mice (4−6 weeks). The mice were kept in a research institution for one week before particle injection. They were randomly assigned to one of five treatment groups: control (n = 10), PEEK particles (n = 10), PE particles (n = 10), PEEK-ZnO particles (n = 10), and PE-ZnO particles (n = 10). Intra-articular injection of wear particles was conducted using a previously reported method [29] (illustrated in Supplementary Material). After one and three months, the mice were sacrificed, and periprosthetic tissue was collected to evaluate the autophagy and inflammation. The collected periprosthetic tissue was first applied to WB and IHC. Next, we isolated the cells from periprosthetic tissues and detected the autophagy flux by treatment with chloroquine and Torin1. The levels of LC3 and ATG16L were evaluated through IFA according to the methods described above.

Wear particles-induced mice calvarial osteolysis model: Mice calvarial osteolysis model was conducted using a previously reported method [29]. Briefly, C57BL/6 mice (6-week-old, male) were anesthetized. The center of the mouse's skull was exposed at the midpoint along the line between the eyes and ears. After the exposure, different wear particles (5 mg/mL, 100 μL per mouse) were implanted near the midline of the skull. The incision was carefully sutured. 2 weeks after the operation, we collected and fixed the cranial bone by 4 % PFA. The bone samples were sectioned after being decalcified in 10 % ethylenediaminetetraacetic acid (EDTA) for 4 weeks. The severity of osteolysis was evaluated by hematoxylin & eosin (H&E) staining, TRAP staining, and micro-CT analysis. The NRecon software was applied to reconstruct the micro-CT images and obtain the following parameters: total volume (TV), bone volume (BV), bone volume/total volume (BV/TV), trabecular number (Tb. N), trabecular thickness (Tb. Th), and trabecular separation (Tb. Sp).

Pathology evaluation of *in vivo* wear particle-induced osteolysis: A pathological osteolysis scoring was performed based on a previously reported scoring system, with mild modification [32]. The criteria included bone response (micro-CT), bone porosity (micro-CT), periosteal resorption, bone formation, and granuloma tissue.

2.4. Statistical analysis

The results and data were presented as mean ± standard deviation (SD). The statistically significant difference between groups was analyzed using a one-way analysis of variance (ANOVA) multiple comparisons conducted by Prism 10 (GraphPad Software, USA). Statistical significance was defined as $P < 0.05$. (*$P < 0.05$. **$P < 0.01$, ***$P < 0.001$, and ****$P < 0.0001$)

3. Results

3.1. Fabrication and characterization of the wear debris

PEEK-ZnO and PE-ZnO composite materials were synthesized by blending PEEK or PE powder with ZnO nanoparticles via high-energy ball milling, followed by compression molding. Fig. 1A illustrates the comprehensive fabrication process. Subsequent evaluations of the elastic modulus and tensile strength of the composites revealed that there were no significant differences between the PEEK and PEEK-ZnO groups nor between the PE and PE-ZnO groups, as depicted in Fig. 1B–D. These findings suggest that the incorporation of ZnO nanoparticles does not compromise the mechanical integrity of the PEEK and PE materials. The surface morphology was examined using SEM, revealing an irregular granular texture in the PEEK-ZnO and PE-ZnO composites (Fig. 1F). EDS analyses further confirmed the successful integration of zinc elements within the PEEK-ZnO and PE-ZnO matrices, as shown in Fig. 1E. These results collectively indicate that ZnO doping can be effectively achieved without detrimentally affecting the fundamental material properties.

Subsequently, wear particles generated from each sample during the wear testing were isolated and analyzed. Initially, the wear particles were examined using SEM and EDS. The particles were found to be irregular in shape with an average diameter of approximately 1 μm, aligning with the findings of our prior research (Fig. 1G). EDS analysis determined the zinc content of the wear particles from the PEEK-ZnO and PE-ZnO samples to be 7.86 % and 8.81 % by weight, respectively (Fig. 1H). Further characterization of the surface chemical composition and bonding states was conducted using XRD and XPS. These techniques provided detailed insights into the structural and chemical properties of the wear particles, enhancing the understanding of their behavior under operational conditions. As shown in Fig. 1I, the FT-IR spectrum showed the characteristic peaks of the PEEK in the PEEK and PEEK-ZnO. The typical peaks included stretching vibration of C=O band at 1652 cm^{-1}, C=C in the benzene ring at 1590 cm^{-1}, in-plane vibration of keto-benzene at 1304 cm^{-1}, asymmetrical stretching vibration of R-O-R at 1226 cm^{-1}, and symmetric vibration of R-CO-R at 929 cm^{-1}. The FT-IR spectrums of PE and PE-ZnO groups both showed characteristic peaks of PE, including asymmetrical and symmetrical stretching vibration of C-H at 2916 and 2847 cm^{-1}. In addition, the PEEK-ZnO and PE-ZnO groups showed evident absorption in the region between 405 and 514 cm^{-1}, identifying the presence of ZnO NPs. Also, the typical orthorhombic crystal structure for the PE and PE-ZnO wear particles was consistent with two peaks indexed at 21.9° and 24.3° in the XRD pattern shown in Fig. 1J. In the PEEK-ZnO and PE-ZnO groups, the reflections observed at 31.8°, 36.3°, 56.6°, 66.4° can be indexed to [100], [101], [110], [102], [112] planes of ZnO. The broad XPS spectra of all samples are shown in Fig. 2K. Furthermore, the high-resolution spectrum of Zn 2p was analyzed. As indicated in Fig. 1L, the peak at 1021 eV was attributed to the Zn 2p, indicating the presence of Zinc in the PEEK-ZnO and PE-ZnO groups. Above all, these results showed that ZnO was successfully doped and did not affect the original mechanical properties and structure.

3.2. Proteomic profiling of synovial fluid in labrador following total hip arthroplasty (THA) using PEEK-HXLPE prostheses

As previously reported, the accumulation of wear particles in the joint cavity may adversely affect several types of cells around the prosthesis. The phagocytosis of wear particles by resident macrophages and other immune cells leads to the secretion of inflammatory factors and the establishment of a local inflammatory microenvironment. In our study, we performed total hip replacement in Labrador dogs with PEEK-on-HXLPE prosthesis. Fig. 2A shows the implanted prosthesis post-operation immediately. Fig. 2B and C shows the joint capsule and the synovial fluid 18 months after the operation. SEM analyzed the PEEK and PE surfaces. As shown in Fig. 2D, after 18 months of implantation,
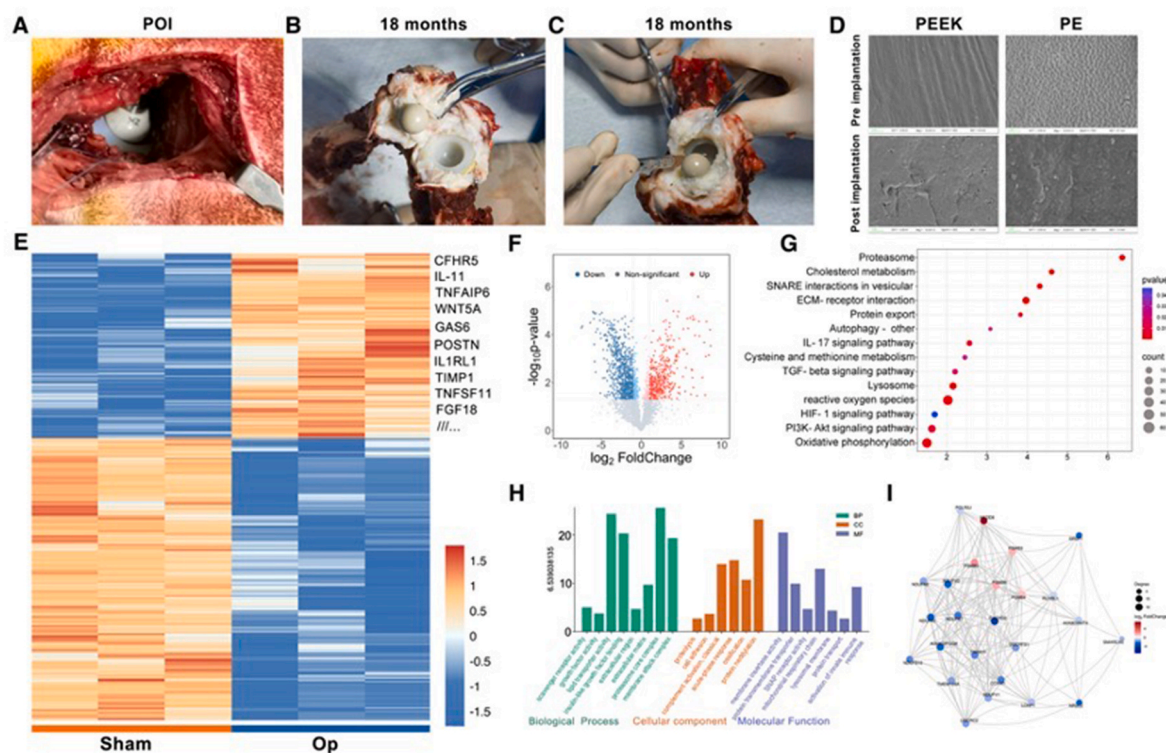
Fig. 2. Proteomic profiling of synovial fluid in Labrador following THA using PEEK-HXLPE prostheses. (A) The implanted PEEK-HXLPE prostheses post-operation immediately. (B–C) The joint capsule and synovial fluid 18 months after the operation. (D) SEM images of the PEEK and PE surfaces before and after the implantation. (E) Microarray heat map visualizing the fold change in expression of proteins. (F) Volcano plots show the expression levels of proteins in different groups. (G) KEGG enrichment analysis result. (H) GO enrichment analysis results classified into biological process (BP), cell composition (CC), and molecular function (MF). (I) Results of protein-protein interaction (PPI) network.

the prosthesis shows different degrees of wear marks, manifesting as scratches, grooves, and pits. The SEM images also reveal the presence of wear particles on the surfaces of the prosthesis.

Furthermore, we collected the synovial fluid for proteomic profiling 18 months after the operation. The proteomic profile of synovial fluid was analyzed by deep data-independent acquisition (DIA) label-free quantitative proteomics analysis. For DIA analysis, 7311 protein groups and 86,341 peptides were detected. We then screened for differentially expressed proteins (DEPs) with the following criteria: $P < 0.05$ and fold change (FC) ≥ 2. As shown in the volcano plot (Fig. 3B), a total of 2056 DEPs were identified in the operation group, compared to the control group, of which 812 were up-regulated, and 1244 were down-regulated. Heat maps of the DEPs were constructed (Fig. 2E). Among the top 20 up-regulated DEPs, the increase in IL1RI, IL11, TNFAIP6, GAS6, WNT5A, and TIMP1 indicated heightened inflammatory activity and may be implicated in tissue remodeling and capsule fibrosis. To further confirm the underlying function of the DEPs, we performed the Gene Ontology (GO) and Kyoto Encyclopedia of Genes and Genomes (KEGG) pathway enrichment analysis and calculated the enrichment score of each term respectively. As shown in Fig. 2G and H, pathways regulating chronic inflammation and immune response were enriched. The IL-17 signaling pathway is directly linked to inflammation by promoting the recruitment of immune cells to the site of inflammation and increasing the production of various inflammatory mediators [33,34]. The enrichment of the PI3K-AKT signaling pathway indicates a likely involvement in promoting inflammation, tissue remodeling, and possibly the presence of capsule fibrosis [35]. Moreover, the KEGG analysis also demonstrated an enrichment of the SNARE interactions in vesicular transport, protein export, and autophagy pathways, which highlights a dynamic and responsive cellular environment within the joint that is actively managing protein trafficking, secretion, degradation, and inflammatory responses. Fig. 2I shows the result of the

protein-protein interaction (PPI) network. The network nodes and the lines correspond to each protein and protein-protein interactions, respectively.

3.3. ZnO doping attenuates the polymer particle-induced inflammation in vitro

Macrophages are the critical cells associated with wear particle-induced inflammation and subsequent osteolysis. We first conducted the CCK-8 assay to investigate the effect of wear particles on macrophage viability. The results showed that RAW264.7 cells viability decreased with wear particle concentration in a dose-dependent manner (Fig. 3A and B). After 12 h and 24 h of treatment, there was a significant decrease in cytotoxicity when the concentration increased to more than 50 μg/mL. Therefore, we confirmed a suitable concentration of wear particles (50 μg/mL) for further stimulation *in vitro*.

The inflammatory reaction provoked by wear particles plays a crucial role in osteolysis and aseptic loosening. *In vitro* analysis has indicated up-regulation of mRNA levels of several pro-inflammatory cytokines and increased secretion of IL-1β, IL-6, and TNF-α [14,36]. Similarly, in tissues collected at the bone–prosthesis interface during surgical revision, increased levels of IL-1β, IL-6, and TNF-α have been observed in direct correlation with the severity of osteolysis[37–40]. Therefore, to evaluate the level of inflammation response and assess whether ZnO doping could mitigate the wear particle-induced inflammation, we measured the mRNA expression of inflammation-associated genes. After 24 h of co-culturing with different groups of wear particles, the expression of both IL-1β and TNF-α was up-regulated compared with the control (Fig. S1). PEEK-ZnO and PE-ZnO groups exhibited a significant decrease in the expression level of IL-1β compared to PEEK and PE groups responsively. However, there were no significant differences among all the particle groups regarding the expression level of TNF-α
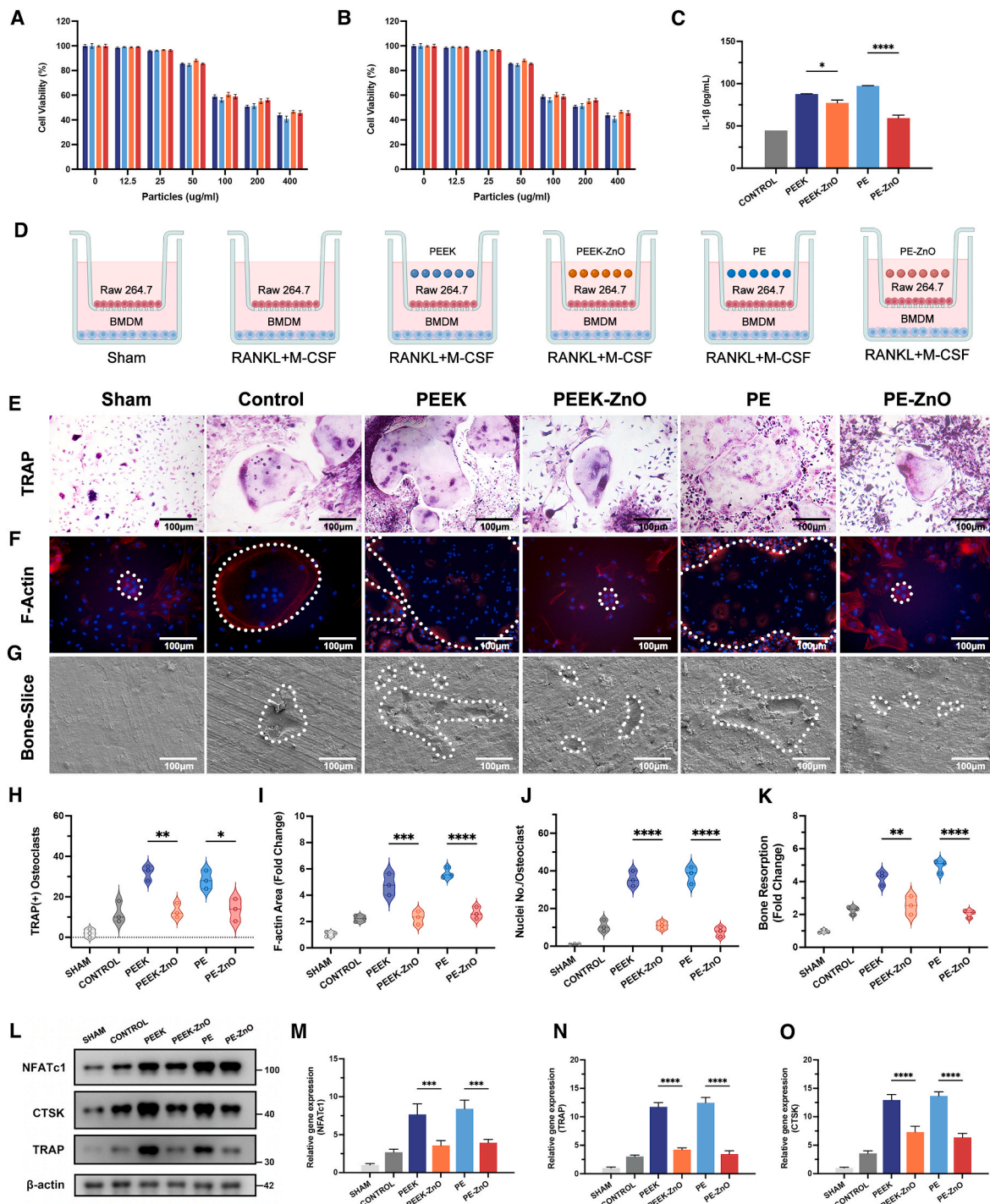
Fig. 3. Assessment of the wear particle-induced inflammation and osteoclastogenesis. (A,B) CCK-8 assay of the RAW264.7 cells co-cultured with wear particles (0, 12.5, 25, 50, 100, 200 and 400 μg/mL) for 12 h and 24 h (n = 3). (C) Quantification of IL-1β protein levels secreted into the cell culture supernatant, as measured by ELISA. All experiments were performed with n = 3 independent biological replicates. (D) Schematic illustration of the double-chamber co-culturing system. (E, F) TRAP and F-actin staining after 7 days of co-culturing (scale bar: 100 μm). (G) Bone slice resorption after 10 days of co-culturing (scale bar: 100 μm). (H) The number of TRAP+ osteoclasts. (I,J) Quantitative analysis of the F-actin area and nuclei numbers of the osteoclasts. (K) Quantitative analysis of the bone resorption area in different groups. (L) Western blot analysis of osteoclastogenesis-related proteins, including NFATc1, CTSK, and TRAP, in BMDMs from each group. (M − O) RT-PCR results of osteoclastogenesis-related genes, including NFATc1, CTSK, and TRAP, in BMDMs from each group. Data are presented as mean ± SD (n = 3). (* indicates P < 0.05, ** indicates P < 0.01, *** indicates P < 0.001, and **** indicates P < 0.0001).

(Fig. S2). We then used ELISA kits to evaluate the levels of IL-1β and TNF-α secreted into the culture supernatant. As shown in Fig. 3C and Fig. S2, the release content of IL-1β and TNF-α were both decreased in the PEEK-ZnO and PE-ZnO groups compared to the PEEK and PE groups. Above all, these results indicated that the ZnO doping reduced pro-inflammatory cytokine secretion and dampened the wear particle-induced inflammation.

3.4. Osteoclastogenesis induced by particle-challenged macrophages can be attenuated by ZnO doping

Once a full-blown inflammatory response is in place, the pro-inflammatory cytokines secreted by the activated macrophages mediate the differentiation of myeloid precursor cells into multi-nucleated osteoclasts and cause bone resorption [41,42]. We designed a double-chamber co-culture system to study the interaction between the activated macrophages and BMDMs under the stimulation of

polymer particles (Fig. 3D). Macrophages were seeded on the porous membrane of the upper chamber and co-cultured with different groups of wear particles, while BMDMs were seeded in the lower chamber. After 10 days of co-culturing under different treatment conditions, the maturation of osteoclasts was detected by TRAP and F-Actin staining. As demonstrated in the TRAP staining and semi-quantification analysis (Fig. 3E,H), the number of TRAP-positive osteoclasts in particle groups was significantly higher than in the control and sham groups. PEEK-ZnO and PE-ZnO groups exhibited a relatively lower number of
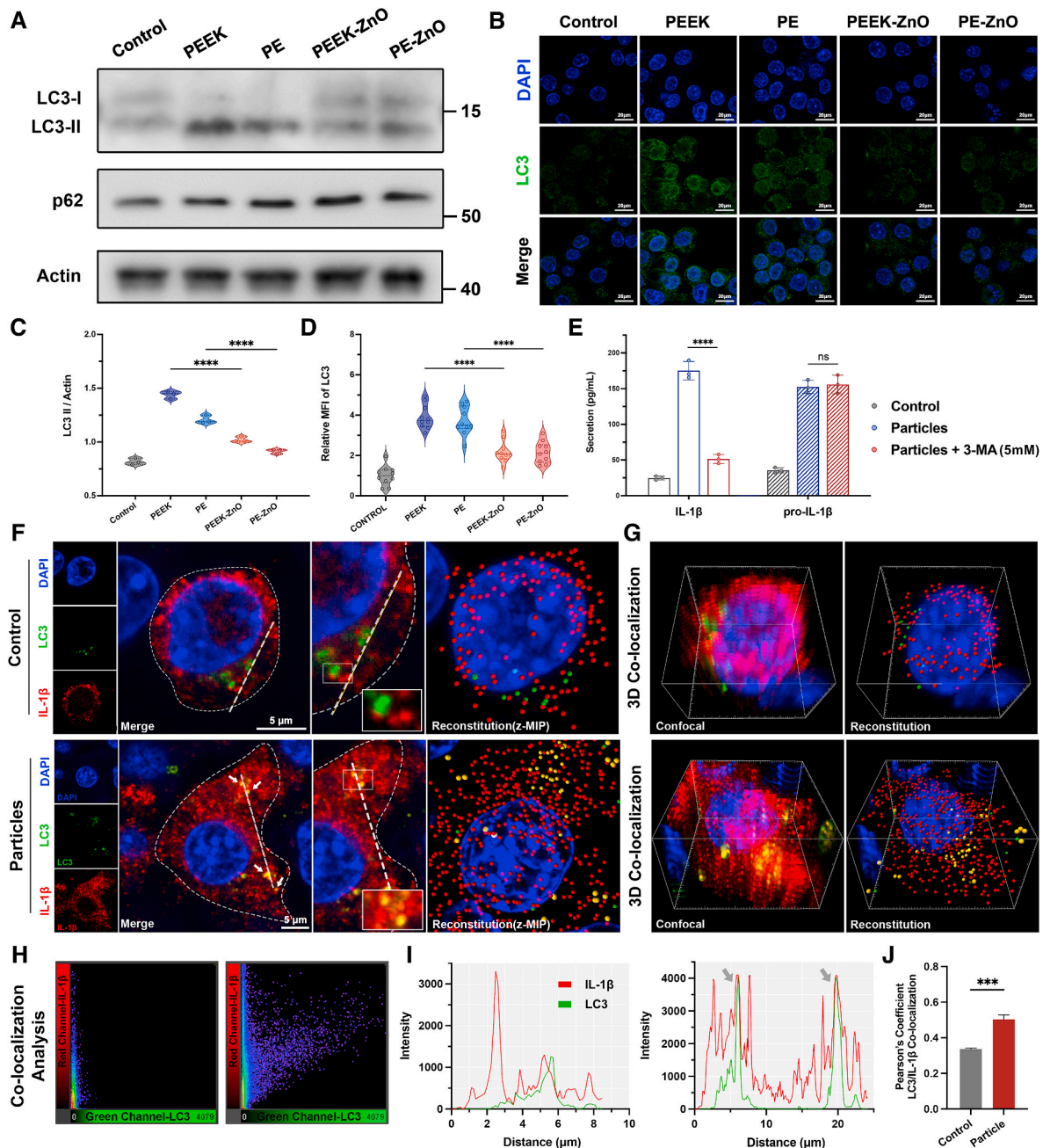

Fig. 4. Autophagy is triggered and mediates the secretion of IL-1β upon stimulation of wear particles. (A, B) WB and immunofluorescence results of autophagy-related proteins in RAW264.7 cells challenged with different wear particles (scale bar: 20 μm). (C) Quantification of LC3-II level in WB. (D) Quantification of LC3 immunofluorescence intensity. (E) Concentrations of IL-1β and pro-IL-1β in culture supernatants of RAW264.7 cells stimulated with wear particles for 12 h in the absence or presence of 3-methyladenine (3-MA) (5 mM). (F) Immunofluorescence staining on RAW264.7 cells and 3D reconstruction for IL-1β (red), LC3 (green), and DAPI (blue) (scale bar: 5 μm). Yellow spots indicate co-localization. (G) 3D co-localization analysis was conducted using the IMARIS coloc plugin. (H) Co-localization analysis of red channel (IL-1β) and green channel (LC3) conducted by FIJI software. (I) Colocalization line tracing analysis from images in (F). Gray arrows indicate the region of red-green overlap. (J) Pearson's colocalization coefficient for IL-1β and LC3. Sample size: n = 3 per group. All experiments were performed with n = 3 independent biological replicates. (ns indicates P > 0.05, *** indicates P < 0.001, and **** indicates P < 0.0001). (For interpretation of the references to colour in this figure legend, the reader is referred to the Web version of this article.)

TRAP-positive osteoclasts than PEEK and PE groups. We then performed phalloidin staining to visualize F-actin rings, a feature of functional osteoclasts. The average F-actin area and nuclei numbers were counted for quantification. As shown in Fig. 3F, I-J, all the particle groups exhibited an increased area of F-actin and number of nuclei. In contrast, PEEK-ZnO and PE-ZnO exhibited a relatively lower number of mature multi-nucleated osteoclasts. These results indicated that under stimulation of the wear particles, the activated macrophages mediated the osteoclastogenesis of BMDMs, and the ZnO doping reduced this process.

One of the most prominent characteristics of functional osteoclasts is their ability to resorb bone. Therefore, we evaluated the bone resorption ability by seeding BMDMs on the bone slices in the lower chamber and measuring the resorption area by SEM after 10 days (Fig. 3G). The results showed that the average resorption area significantly increased upon the stimulation of wear particles. Similar to the results of osteoclastogenesis evaluation, the average bone resorption area in the PEEK-ZnO and PE-ZnO groups decreased significantly compared to the PEEK and PE groups (Fig. 3K).

Moreover, the findings of osteoclast-related genes and protein expression (TRAP, cathepsin K, NFATc1) assays revealed that exposure to the conditioned medium collected from macrophages in the PEEK-ZnO and PE-ZnO group resulted in significant suppression of osteoclast differentiation and maturation compared with that collected from cells in the PEEK and PE groups (Fig. 3L–O).

In summary, wear particles stimulated the macrophages to mediate the osteoclast differentiation. Wear particles from the ZnO-doped PEEK and PE materials showed inhibitory effects on osteoclastogenesis and alleviated bone resorption, indicating that ZnO doping attenuated bone resorption under wear particle-induced inflammation.

3.5. Secretory autophagy mediates the secretion of IL-1β upon stimulation of wear particles

A growing body of evidence has confirmed that autophagy, as a survival mechanism in response to various stresses, is triggered by the presence of wear particles and accelerates the process of wear particle-induced osteolysis[23–25]. 3-Methyladenine (3-MA) treatment reduced TNF-α secretion in macrophages stimulated by Tips[31]. To investigate the effect of different wear particles on macrophage autophagy, we co-cultured macrophages with wear particles and analyzed the autophagy marker. Western blot assay was performed to determine the expression levels of autophagosome protein (LC3) and autophagy substrate protein (p62). As shown in Fig. 4A, the protein level of LC3 was significantly increased in particle-stimulated macrophages. PEEK-ZnO and PE-ZnO groups showed relatively decreased LC3 levels compared to the PEEK and PE groups. Immunofluorescence experiments and quantification assay of LC3 yielded similar results, indicating that autophagy was triggered in macrophages by wear particles, and ZnO doping exhibited an inhibitory effect (Fig. 4B–D).

Based on the autophagy mechanism involved in cellular stress response, it was anticipated that the presence of wear particles would trigger autophagy. Moreover, according to a number of studies, autophagy mediates the secretion of inflammatory cytokine in a cell process called secretory autophagy [26,27,43,44]. Upon cellular stresses such as starvation and oxidative stress, mature IL-1β is sequestered into autophagosomes and subsequently trafficked to the plasma membrane for secretion [45]. Secretory autophagy may constitute a key mechanism in aseptic loosening pathology. To further investigate the relation between macrophage inflammation response and autophagy, we assessed the IL-1β and pro-IL-1β secretion of macrophages at different levels of autophagy. As shown in Fig. 4E, autophagy inhibition by 3-MA (5 mM) significantly reduced the macrophage secretion of IL-1β upon stimulation of wear particles. The results indicated that autophagy has a regulatory effect on wear particle-induced inflammation. However, secreted pro-IL-1β levels observed in PEEK-ZnO and PE-ZnO were not reduced by 3-MA. Moreover, 3-MA neither modulated intracellular IL-1β nor

pro-IL-1β levels. These data suggest that autophagy-mediated the IL-1β secretion of particle-stimulated macrophage but did not affect pro-IL-1β secretion. This leads us to hypothesize that secretory autophagy may play a crucial role in the wear particles-induced inflammation response.

In order to validate the requirement of autophagy for the translocation of cytosolic IL-1β to a vesicular compartment that could be subsequently conducted by membrane fusion to the extracellular medium, we investigated and analyzed the intracellular distribution of IL-1β. To evaluate whether IL-1β colocalizes with the autophagy marker LC3, we conducted confocal immunofluorescence microscopy 12 h after the stimulation of wear particles (Fig. 4F). The 3D co-localization results showed that when the macrophages were co-cultured with wear particles, overlap between LC3 and IL-1β was observed, indicating the LC3/IL-1β colocalization (Fig. 4G–J). Overall, these results indicated that autophagic organelles and IL-1β intersect upon stimulation of wear particles, and inhibition of autophagy flux reduced the IL-1β secretion.

3.6. ZnO doping inhibits the autophagy-mediated IL-1β secretion

The results presented above demonstrate the involvement of autophagy in the process of IL-1β secretion following stimulation by wear particles [46,47]. ZnO doping showed an inhibitory effect on autophagy, which agrees with previous studies. It has been reported that ZnO NPs are known to cause blockage of autophagy flux in A549 cells, which is primarily attributed to lysosomal impairment [34]. Liu et al. reported that ZnO nanoparticles blocked autophagy flux due to impaired microtube disruption and impaired fusion process of autophagosomes and lysosomes [48]. Combining the previous results, it is expected that ZnO NPs may interfere with the wear particle-induced IL-1β secretion. Therefore, we performed further experiments to investigate the co-localization level of LC3 and IL-1β upon the stimulation of different wear particles. After stimulation by different groups of wear particles, the fluorescence intensity of both LC3 and IL-1β was increased (Fig. 5B and C). Compared to PEEK and PE groups, the expression level of LC3 in ZnO-doped groups was decreased, while no static difference was observed in the intracellular IL-1β expression. These results were consistent with the previous experiments. To quantify the degree of colocalization between IL-1β and LC3B, we performed whole-cell 3D CLSM and reconstructed the CLSM images to conduct a 3D co-localization analysis. As shown in Fig. 5A, PEEK and PE groups exhibited high levels of co-localization, while PEEK-ZnO and PE-ZnO groups exhibited relatively lower levels of co-localization. Following the reconstruction, Manders' coefficients of different groups were calculated (Fig. 5D). The results showed that Manders' coefficients significantly increased after the stimulation of wear particles and underwent a reduction in PEEK-ZnO and PE-ZnO groups compared to PEEK and PE groups. These observations, along with the previous results that ZnO doping reduced IL-1β secretion, suggested that ZnO-doped wear particles lower the co-localization level of LC3 and IL-1β, which inhibits the process of autophagy-mediated IL-1β secretion and may attenuate the wear particle-induced inflammation.

3.7. R-SNARE Sec22b and TRIM16 are involved in autophagy-mediated IL-1β secretion

Recent studies have unraveled the mechanism of secretory autophagy [44,49]. Upon lysosomal damage caused by various stimulations, the activation of the inflammasome leads to the maturation of cytosolic IL-1β, which is dependent on caspase-l. (Scheme 1A) As highlighted in recent literature, including the study by Nguyen, TRIM16, in conjunction with Sec22b, captures cytosolic mature IL-1β and facilitates its incorporation into LC3-positive vesicles [45]. These vesicles are then directed toward the plasma membrane, where IL-1β is released into the extracellular space through the action of specific SNARE proteins such as syntaxin 3/4 and SNAP23/29. To further confirm the role of secretory autophagy in the context of IL-1β secretion, we performed a
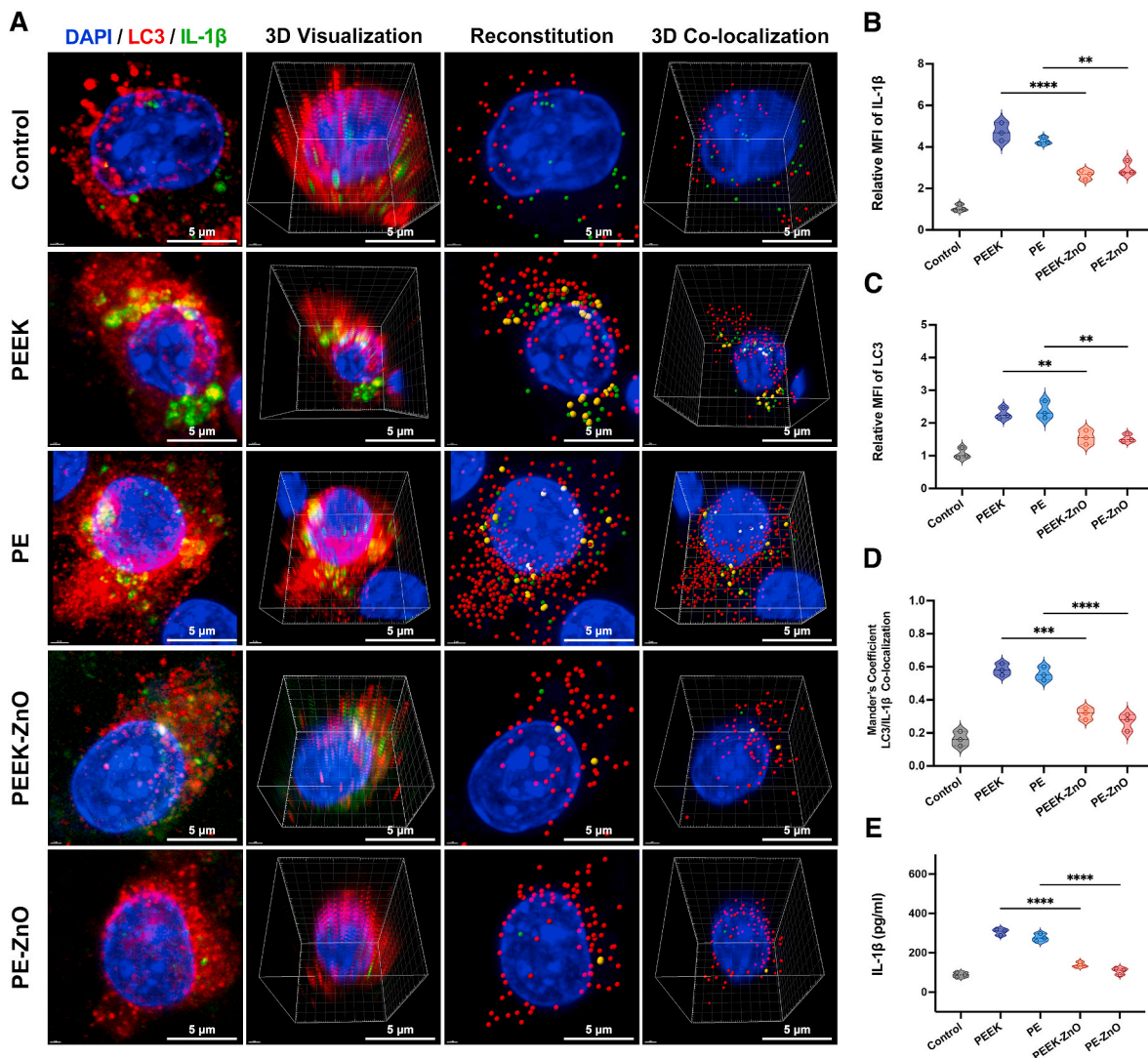
Fig. 5. ZnO doping inhibits the autophagy-mediated IL-1β secretion. (A) Immunofluorescence staining on RAW264.7 cells for IL-1β (red), LC3 (green), and DAPI (blue) after treated with different wear particles (scale bar: 5 μm). (B, C) Quantification of IL-1β and LC3 immunofluorescence intensity. (D) Mander's co-localization coefficient of LC3 and IL-1β. (E) Concentrations of IL-1β in culture supernatants of RAW264.7 cells stimulated with different wear particles. Sample size: n = 3 per group. All experiments were performed with n = 3 independent biological replicates. (** indicates P < 0.01, *** indicates P < 0.001, and **** indicates P < 0.0001). (For interpretation of the references to colour in this figure legend, the reader is referred to the Web version of this article.)

co-localization analysis of LC3/Sec22b and LC3/TRIM16. As shown in Fig. 6A–E, 3D-colocalization CLSM results evidenced a significant increase in the co-localization of LC3 and TRIM16 after being stimulated with wear particles. This result suggested that TRIM16 may bind IL-1β as a secretory autophagy cargo. Moreover, our results showed an evident co-colocalization of Sec22b and IL-1β after particle stimulation (Fig. 6F–J), indicating that TRIM16 binding IL-1β can form a complex with Sec22b to transfer the cargo to the LC3-positive vesicles for secretion. The hypothesized mechanism of the autophagy-mediated IL-1β secretion is presented in Scheme 1B.

3.8. Autophagic flux and inflammation assessment of wear particles-induced inflammation in vivo

Wear particles were generated and released into the joint capsule and bone-implant interfaces, leading to local inflammation of the joint synovium and the periprosthetic membrane. The cellular component of the surrounding tissue includes fibroblast-like synoviocytes, macrophages, osteoclasts, and less frequently mesenchymal cells (MSCs) [50]. The majority of these cells can phagocyte the wear particles and release

various pro-inflammatory cytokines in response. To evaluate the autophagy and inflammation levels of the periprosthetic tissue, we constructed an animal model of wear particle injection. Fig. 7A illustrates the general procedure of the animal model. Different groups of wear particles were implanted into the knee joint capsule of the mouse. Periprosthetic tissue was collected 1 month after the implantation to evaluate the autophagy and inflammation in the early stage. We first performed an autophagy flux detection on the normal synovial cells. Treatment with Torin1, an inhibitor of mTOR that stimulates autophagy, up-regulated the level of LC3 and reduced the level of p62. Next, the lysosome inhibitor chloroquine (CQ) was used to block autophagic degradation. As expected, the protein levels of LC3 and p62 were both significantly increased (Fig. 7B). In addition, we evaluated the expression level of several autophagy marker proteins by immunofluorescence, including LC3, ATG16L, FIP200, and WIPI2 (Fig. 7C). These results suggested that the autophagic flux of the normal synovial cells was unobstructed.

We then performed a Western blot analysis on the periprosthetic tissue lysates and observed a similar trend with the previous *in vitro* experiments (Fig. 7D, F-G). The stimulation of wear particles increased
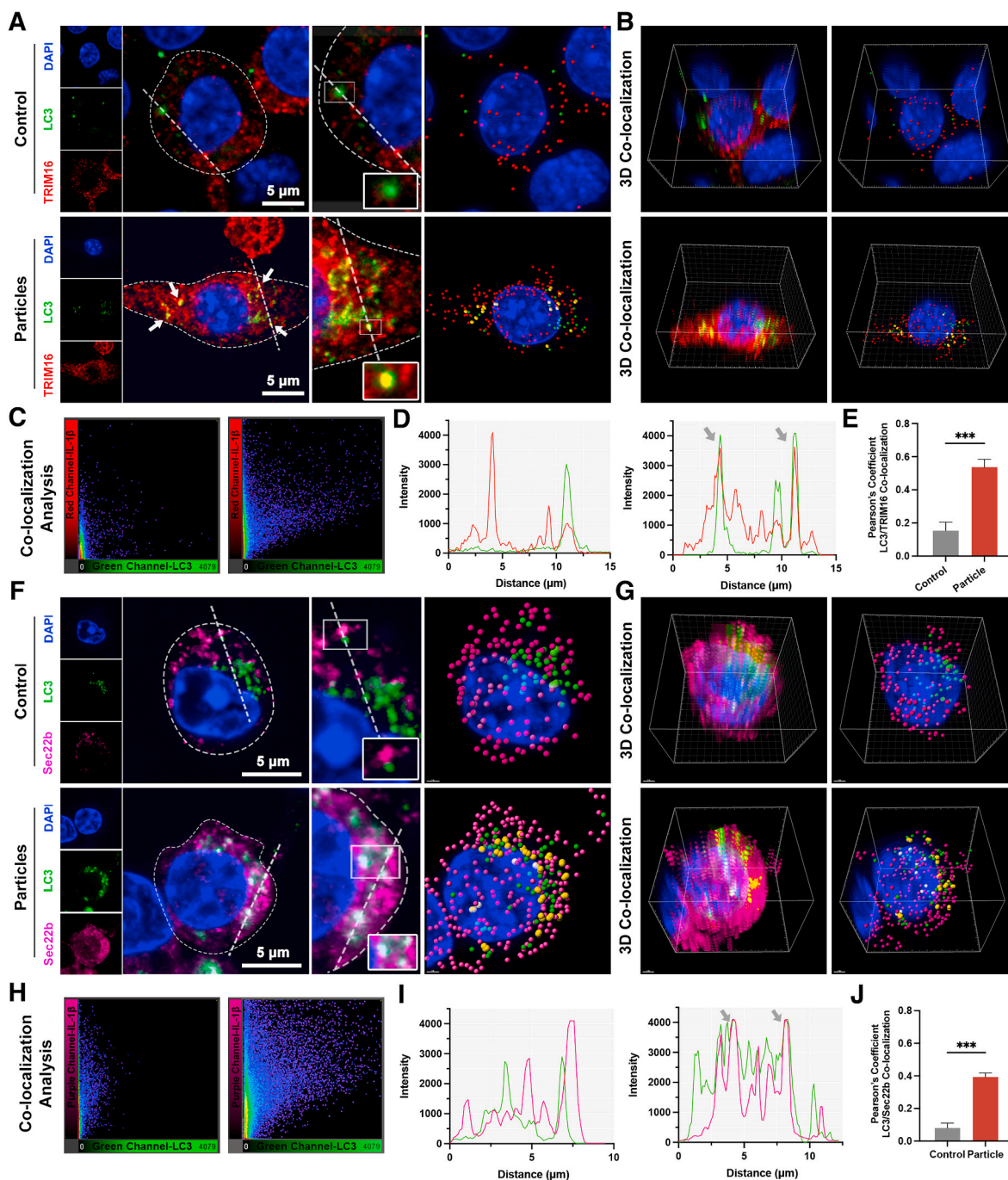
Fig. 6. Sec22b and TRIM16 are involved in autophagy-mediated IL-1β secretion. (A) Immunofluorescence staining on RAW264.7 cells and 3D reconstruction for TRIM16 (red), LC3 (green), and DAPI (blue) (scale bar: 5 μm). Yellow spots indicate co-localization. (B) 3D co-localization analysis conducted by IMARIS coloc plugin. (C) Co-localization analysis of red channel (TRIM16) and green channel (LC3) conducted by FIJI software. (D) Colocalization line tracing analysis from images in (A). Gray arrows indicate the region of red-green overlap. (E) Pearson's colocalization coefficient for TRIM16 and LC3. (F) Immunofluorescence staining and 3D reconstruction for Sec22b (purple), LC3 (green), and DAPI (blue) (scale bar: 5 μm). White spots indicate co-localization. (G) 3D co-localization analysis conducted by IMARIS coloc plugin. (H) Co-localization analysis of purple channel (TRIM16) and green channel (LC3) conducted by FIJI software. (I) Colocalization line tracing analysis from images in (F). Gray arrows indicate the region of purple-green overlap. (J) Pearson's colocalization coefficient for Sec22b and LC3. Sample size: n = 3 per group. All experiments were performed with n = 3 independent biological replicates. (*** indicates $P < 0.001$). (For interpretation of the references to colour in this figure legend, the reader is referred to the Web version of this article.)

the protein level of LC3, and ZnO-doped groups exhibited lower levels of LC3. Meanwhile, the protein levels of p62 in PEEK-ZnO and PE-ZnO groups were relatively higher than those in PEEK and PE groups, respectively. Similarly, the immunohistochemistry (IHC) stain of tissue sections demonstrated a lower level of LC3 expressed in PEEK-ZnO and PE-ZnO compared to the PEEK and PE groups (Fig. 7E). These results

may be due to the blocking effect of ZnO doping on the autophagic flux.

Furthermore, we assessed the expression of autophagy marker protein LC3 and ATG16L. The cells were dissociated from the periprosthetic tissues and treated with Torin1 and Torin1+CQ to reflect the actual level of autophagic flux. As shown in Fig. 7I–L, PEEK-ZnO, and PE-ZnO groups showed a lower expression of LC3 and ATG16L, indicating that ZnO
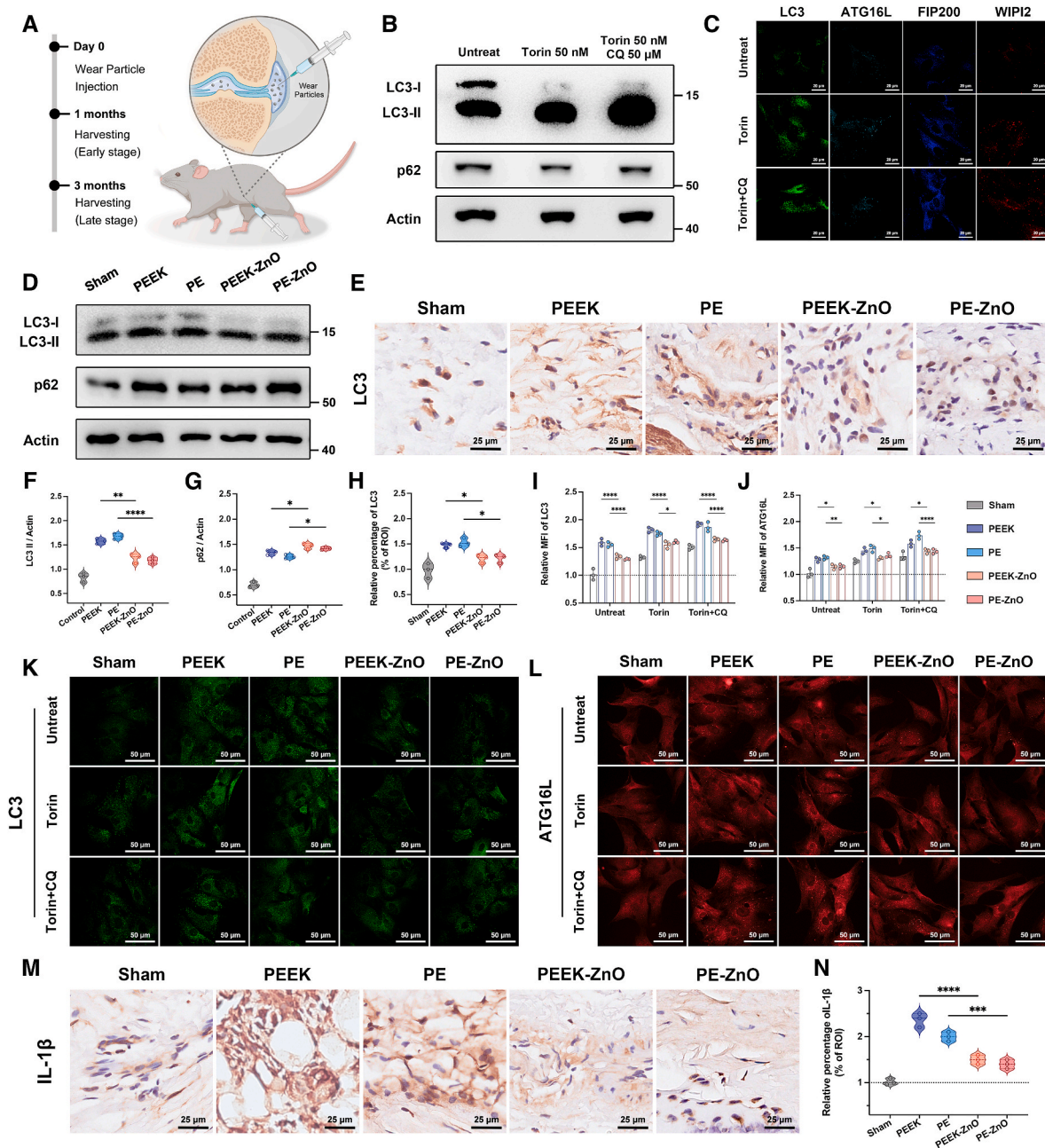
Fig. 7. Autophagic flux and inflammation assessment *in vivo*. (A) Schematic illustration of intra-articular injection of prosthetic wear particles. (B) WB result of autophagy flux in normal synovial cells treated with Torin (50 nM) and Torin (50 nM) + CQ (50 μM) for 4 h. (C) Immunofluorescence staining on normal synovial cells for LC3 (green), ATG16L (cyan), FIP200 (blue), and WIPI2 (red) (scale bar: 20 μm). (D) WB results of autophagy-related proteins in the periprosthetic tissue lysates. (E) IHC staining results for LC3 of the periprosthetic tissue section (scale bar: 25 μm). (F, G) Quantification of LC3-II and p62 level in WB result (D). (H) IHC quantification for LC3. (I, J) Quantification of fluorescence intensity of LC3 and ATG16L. (K, L) Immunofluorescence staining on the isolated synovial cells for LC3 and ATG16L after treatment of Torin (50 nM) and Torin (50 nM) + CQ (50 μM) for 4 h (scale bar: 50 μm). (M, N) IHC staining and quantification results for IL-1β of the periprosthetic tissue section (scale bar: 25 μm). Sample size: n = 3 per group. All experiments were performed with n = 3 independent biological replicates. (* indicates $P < 0.05$, ** indicates $P < 0.01$, *** indicates $P < 0.001$, and **** indicates $P < 0.0001$). (For interpretation of the references to colour in this figure legend, the reader is referred to the Web version of this article.)

doping inhibited the autophagic flux of the periprosthetic tissues upon particle stimulation. To evaluate the local inflammation of periprosthetic tissues, we collected and stained the histological sections with IHC. The results of IHC staining and quantitative analysis are shown in Fig. 7M and N. The decreased level of IL-1β and TNF-α in PEEK-ZnO and PE-ZnO groups indicates that ZnO doping attenuated the local inflammation induced by wear particles *in vivo*.

To further investigate the autophagy and inflammation levels in the late stage, we collected the periprosthetic tissues three months after the

implantation of wear particles. The periprosthetic tissues were homogenized for WB analysis. As shown in Fig. S1A, the protein level of LC3 in the PEEK and PE groups was still up-regulated after three months. By contrast, the PEEK-ZnO and PE-ZnO groups showed a similar level of LC3 to the sham group. We then dissociated the synovial cells from the periprosthetic tissues and evaluated the autophagic flux. The PEEK-ZnO and PE-ZnO groups exhibited decreased levels of LC3 compared to the PEEK and PE groups, which were similar to the autophagy level of the sham groups (Fig. S3B). Moreover, we stained the histological sections

with IHC to evaluate the level of IL-1β. There was a significant decrease in the level of IL-1β in the PEEK-ZnO and PE-ZnO groups compared to the PEEK and PE groups (Figs. S3C and D). Finally, we also performed an *in vivo* bio-safety test based on the histology of the major organs via H&E staining. The results showed that there is no significant side effect on these organs after treatment of ZnO-doped wear particles (Fig. S4). These results indicated that the inhibition of autophagic flux by ZnO doping was relieved in the late stage of wear particle implantation. The ZnO doping exerted a moderate and transient regulatory effect on the autophagy level of the periprosthetic tissues and did not cause long-term cytotoxicity.

3.9. Protective effects of ZnO doping on wear particle-induced mice calvaria osteolysis

To further evaluate the effect of the ZnO doping on wear particle-induced osteolysis *in vivo*, we conducted a calvaria osteolysis model and implanted PEEK, PE, PEEK-ZnO, and PE-ZnO wear particles (Fig. 8A). Fig. 8A illustrated the wear particle-induced calvaria osteolysis model. As demonstrated in Fig. 8E, the severity of osteolysis is significantly increased after stimulation of different wear particles. The bone parameters of the wear particle group, including BV/TV, Tb. N, and TB. Th, were also significantly increased (Fig. 8B–D). By contrast, PEEK-

ZnO and PE-ZnO groups exhibited significantly decreased osteolysis severity. Moreover, we performed H&E and TRAP staining and evaluated the histological changes in the bone structure. As shown in Fig. 8F and G, the calvaria tissue structure is more severely damaged, and the typical bone microstructure is lost, with the most TRAP$^+$ osteoclasts observed in the PEEK and PE groups. By contrast, in the PEEK-ZnO and PE-ZnO groups, the severity of bone damage and the number of TRAP$^+$ osteoclasts were significantly decreased (Fig. 8H). Furthermore, pathological osteolysis scoring was performed based on bone response (micro-CT), bone porosity (micro-CT), periosteal resorption, bone formation, and granuloma tissue (Fig. 8I and J). Compared with PEEK and PE groups, the average osteolysis score of PEEK-ZnO and PE-ZnO was significantly decreased, suggesting that ZnO doping effectively attenuated the particle-induced osteolysis *in vivo*.

4. Discussion

Wear particles from various materials, including CoCrMo, titanium, ultra-high molecular weight polyethylene (UHMWPE), PEEK, and XLPE, have been generally considered the leading cause of periprosthetic osteolysis and aseptic loosening. Although all prosthesis materials potentially generate wear particles and induce bone resorption with various biological mechanisms, polymer wear particles are the most
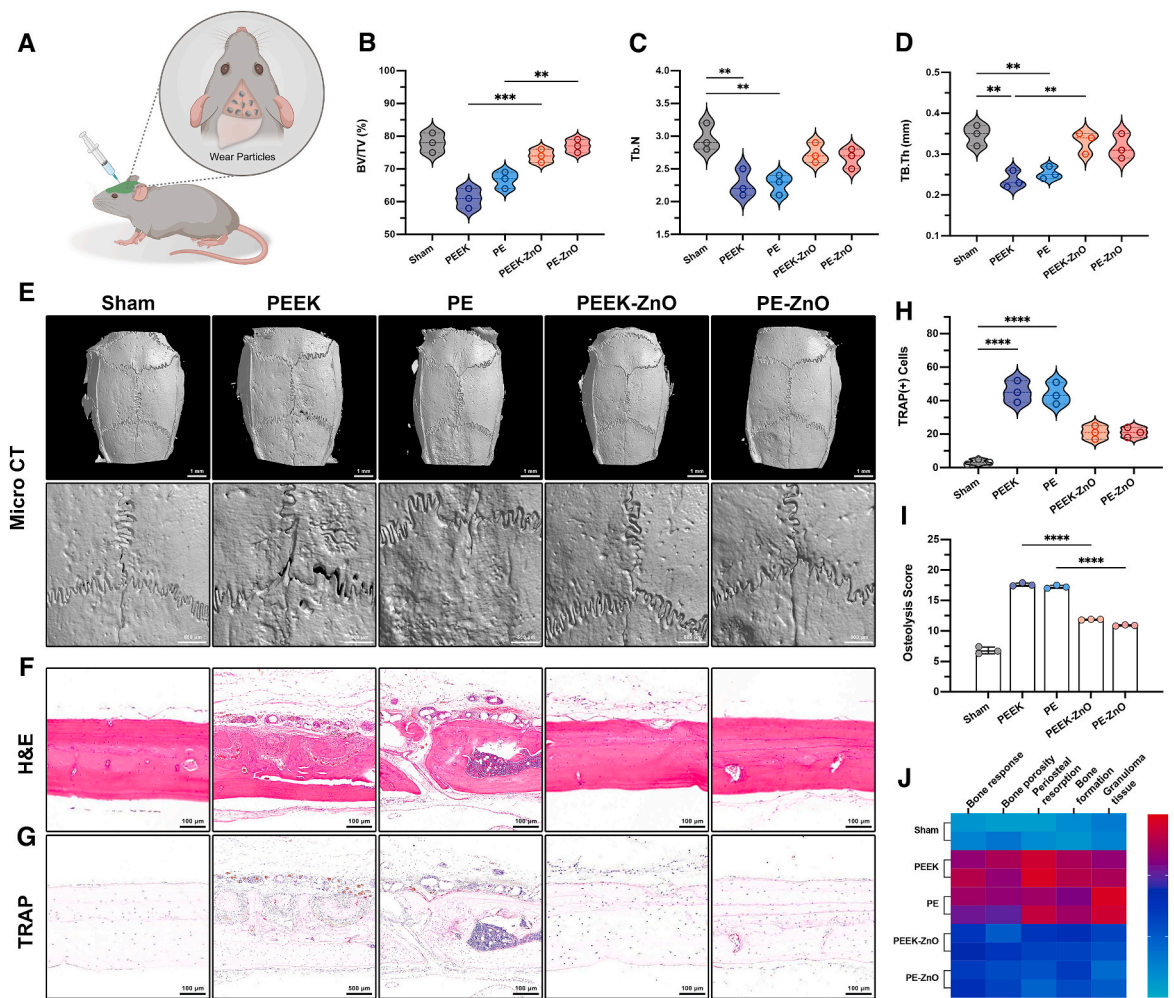

Fig. 8. Protective effects of ZnO doping on wear particle-induced mice calvaria osteolysis. (A) Schematic illustration of wear particle-induced mice calvaria osteolysis model. (B–E) Micro-CT analysis and relevant parameters for wear particles-induced osteolysis in mice calvaria (scale bar: 100 μm). Analysis was performed with n = 3 independent experiments. (F) H&E staining in different groups (scale bar: 100 μm). (G) TRAP staining in different groups (scale bar: 100 μm; arrows represent TRAP-positive cells). (H) The number of TRAP-positive cells in different groups. (I–J) Osteolysis score of different groups. (* indicates P < 0.05, ** indicates P < 0.01, *** indicates P < 0.001, and **** indicates P < 0.0001).

abundant in the joint and are, therefore, likely to be the most significant wear particles in the joint replacement system [7,51]. Therefore, this study focused on the effects of polymer (PEEK and PE) wear particles. In addition, the design characteristics of this study on the interaction between polymer particles and macrophages were consistent with previously published clinical studies, as well as *in vitro* and *in vivo* experiments [52]. Thus, the polymer wear particles studied in this work may provide a relatively accurate simulation of wear particle-induced inflammation and osteolysis.

Skeletal homeostasis depends on the balanced action of bone-resorbing osteoclasts and bone-forming osteoblasts. Disruption of this balance can lead to skeletal disorders. In the context of periprosthetic osteolysis, wear particles from joint prostheses activate macrophages, leading to the secretion of pro-inflammatory cytokines. This creates a pro-inflammatory microenvironment that disrupts the equilibrium between bone resorption and formation, favoring osteolysis. To investigate this phenomenon further, we conducted a study where synovial fluid was collected from the hip joints of Labrador dogs 18 months post-total hip arthroplasty for proteomic analysis. This approach allowed us to profile the protein constituents that potentially contribute to the inflammatory processes associated with periprosthetic osteolysis. The result of the top 20 increased DEPs did not reveal significant elevations in canonical inflammatory cytokines such as IL-1β, IL-6, and TNF-α, which are typically up-regulated during acute and initial inflammatory phases. This may be attributed to the later stage of the inflammatory response in our THA models, as well as the varied tissue distribution of these inflammatory mediators. Nonetheless, the identification of increased levels of IL1RI, IL11, TNFAIP6, GAS6, WNT5A, and TIMP1 still indicates a continuous and active state of inflammation. Correspondingly, histological examination, as shown in Fig. 2B, revealed marked thickening and fibrosis in the joint capsule. Given that fibrosis is commonly linked with chronic and dysregulated inflammatory processes, this result also supported the notion of wear particle-induced inflammation within the joint. Moreover, further insights were provided by the KEGG analysis, which highlighted significant enrichment in pathways associated with SNARE interactions in vesicular transport, protein export, and autophagy. These findings underscore a highly dynamic and responsive cellular environment in the joint, engaged in intricate mechanisms of protein trafficking, secretion, degradation, and modulation of inflammatory responses. This complex cellular activity is crucial for managing the ongoing inflammatory state triggered by wear particles.

Autophagy, a cellular mechanism for the degradation and recycling of damaged components, is pivotal in bone remodeling. It plays an essential role in the differentiation of osteoblasts and osteoclasts, contributing to mineralization and the maintenance of bone homeostasis. Additionally, autophagy is crucial for the survival of osteocytes and is thereby implicated in the overall integrity of bone tissue. Recent studies have underscored the significance of autophagy in the context of wear particle-induced osteolysis. It has been demonstrated that autophagy is activated upon exposure to wear particles, which in turn accelerates osteolytic processes [24,25]. For example, Wang et al. observed that autophagy-mediated the effects of CoCrMo wear particles by promoting apoptosis in osteoblasts, while TiAl6V4 particles were found to enhance osteoclast formation through an autophagy-dependent downregulation of interferon-beta in osteocytes [22]. In our investigations, we found that macrophages phagocytose polymer wear particles (PEEK and PE), leading to an upregulation of autophagy. Subsequent stimulation by these particles triggered increased autophagic activity in both macrophages and periprosthetic tissues, which was associated with heightened inflammation and the progression of osteolysis. This evidence suggests that modulating autophagy in the peri-implant environment could be a potential strategy for mitigating wear particle-induced bone degradation. Beyond its traditional role in protein degradation, emerging evidence suggests that autophagy also facilitates the unconventional secretion of leaderless proteins through a mechanism termed secretory autophagy. This process becomes particularly critical during immune system disturbances caused by inflammation or infection, wherein autophagy machinery may reroute part of its cargo to exosomes. These exosomes act as messengers, conveying vital information to neighboring cells and thus enhancing immune responsiveness to potential threats. The role of secretory autophagy could be fundamental in the pathology of aseptic loosening.

In this context, our study aimed to explore whether secretory autophagy is implicated in the inflammatory response induced by wear particles. We observed that upon exposure to wear particles, IL-1β was localized to autophagic compartments, evidenced by its colocalization with the autophagy marker LC3, as assessed through CLSM. Moreover, we found that inhibiting autophagy with 3-MA significantly diminished the secretion of IL-1β triggered by wear particles. These findings substantiate the involvement of secretory autophagy in mediating the release of IL-1β in response to wear particle stimulation, highlighting its potential as a therapeutic target in mitigating wear particle-induced inflammatory responses.

Recent studies have unraveled the detailed mechanism of secretory autophagy [44,49]. Upon lysosomal damage caused by various stimulations, the activation of the inflammasome leads to the caspase-l-dependent maturation of cytosolic IL-1β. Glycosylated lysosomal lumenal proteins are released into the cytosol and activate the Gal-8–TRIM16 complex. TRIM16 works in conjunction with its binding partner Gal-8 to capture cytosolic mIL-1β. This complex then combines with Sec22b and is incorporated into LC3-positive vesicles, which are directed toward the plasma membrane for secretion. In our study, the co-localization of TRIM16/LC3 and Sec22 b/LC3 was observed by CLSM and 3D co-localization analysis, which further confirmed that the secretory autophagy pathway is involved in the pathogenesis of wear particle-induced inflammation and osteolysis. Moreover, it is predicted that interventions targeting autophagy in activated macrophages challenged by wear particles are crucial for attenuating periprosthetic osteolysis.

ZnO has various medical applications thanks to its biocompatibility and intrinsic anti-inflammatory and antimicrobial activity [53,54]. Our previous study found that ZnO NPs effectively reduced inflammation and bone loss caused by PEEK and PE particles by inhibiting MEK and ERK phosphorylation and reducing COX-2 expression [29]. Previous research has also reported that Zinc can regulate macrophage polarization and establish an anti-inflammatory environment [28]. Moreover, Zinc has been reported to stimulate osteoblast bone formation, increase alkaline phosphatase (ALP) activity, and inhibit osteoclast differentiation. With these distinct properties, Zinc plays a critical role in bone remodeling and regeneration processes. In this study, we modified the bulk composition of the polymer materials by doping a trace amount of ZnO NPs before the molding process. According to the results from *in vivo* and *in vitro* experiments, the PEEK-ZnO and PE-ZnO materials exhibited lower levels of autophagy and inflammatory reaction. Our findings indicated that ZnO doping may inhibit the over-stimulated autophagy and possess a protective effect on the wear particle-induced inflammation and osteolysis. However, the results should be treated with caution due to the various intrinsic properties of ZnO in bone remodeling. Multiple mechanisms are involved in the pathogenesis of wear particle-induced osteolysis and may interact with the protective effects of ZnO doping. The exact role of ZnO doping in wear particle-induced inflammation and osteolysis warrants further investigation.

While our study provides valuable insights into the role of autophagy in wear particle-induced inflammation and osteolysis, several limitations should be acknowledged. First, the interplay between classical autophagy, which is known to mediate the degradation of IL-1β, and secretory autophagy, which facilitates IL-1β secretion, remains complex and not fully understood. The balance between these two pathways may influence the overall inflammatory response, and further research is needed to elucidate how they interact under different pathological

conditions. Additionally, although our study focused on IL-1β as a key mediator of osteoclastogenesis, other factors such as TNF-α, which also play critical roles in bone resorption, were not extensively explored. The impact of ZnO doping on the regulation of TNF-α and other inflammatory cytokines warrants further investigation to provide a more comprehensive understanding of the mechanisms at play. In future research, it will be important to delve deeper into these aspects, particularly to clarify the interactions between different autophagic pathways and to assess the broader spectrum of cytokines involved in wear particle-induced osteolysis.

In summary, our research provides unique insights into the pathogenic mechanisms of wear particle-induced inflammation and osteolysis. Considering the inevitability of prosthesis wear due to material limitations, strategies aimed at enhancing the biological response to wear particles appear more viable. Consequently, our study not only sheds light on innovative modification methods for prosthesis materials but also underscores the promising potential of ZnO-doped prostheses. These modifications are intended to mitigate the inflammatory osteolysis triggered by wear particles, offering a significant advancement in prosthetic technology and patient outcomes.

Funding

Data and materials availability

All data are available in the main text or the Supplementary Material.

CRediT authorship contribution statement

Zhuocheng Lyu: Investigation, Writing – review & editing, Writing – original draft. **Xiangchao Meng:** Methodology. **Fei Hu:** Methodology, Visualization. **Yuezhou Wu:** Data curation. **Yurun Ding:** Investigation. **Teng Long:** Methodology, Investigation. **Xinhua Qu:** Supervision, Writing – review & editing. **You Wang:** Writing – review & editing, Supervision, Conceptualization.

Declaration of competing interest

The authors declare that they have no known competing financial interests or personal relationships that could have appeared to influence the work reported in this paper.

Data availability

Data will be made available on request.

Appendix A. Supplementary data

Supplementary data to this article can be found online at https://doi.org/10.1016/j.mtbio.2024.101225.

References

[1] J. Gao, D. Xing, S. Dong, J. Lin, The primary total knee arthroplasty: a global analysis, J. Orthop. Surg. Res. 15 (2020) 190, https://doi.org/10.1186/s13018-020-01707-5.

[2] I. Shichman, M. Roof, N. Askew, L. Nherera, J.C. Rozell, T.M. Seyler, R. Schwarzkopf, Projections and epidemiology of primary hip and knee arthroplasty in medicare patients to 2040-2060, JBJS Open Access 8 (2023), https://doi.org/10.2106/JBJS.OA.22.00112.

[3] N.A. Hodges, E.M. Sussman, J.P. Stegemann, Aseptic and septic prosthetic joint loosening: impact of biomaterial wear on immune cell function, inflammation, and infection, Biomaterials 278 (2021) 121127, https://doi.org/10.1016/j.biomaterials.2021.121127.

[4] S.B. Goodman, J. Gallo, Periprosthetic osteolysis: mechanisms, prevention and treatment, JCM 8 (2019) 2091, https://doi.org/10.3390/jcm8122091.

[5] R.T. Beck, K.D. Illingworth, K.J. Saleh, Review of periprosthetic osteolysis in total joint arthroplasty: an emphasis on host factors and future directions, J. Orthop. Res. 30 (2012) 541–546, https://doi.org/10.1002/jor.21554.

[6] J.J. Cherian, J.J. Jauregui, S. Banerjee, T. Pierce, M.A. Mont, What host factors affect aseptic loosening after THA and TKA? Clin. Orthop. Relat. Res. 473 (2015) 2700–2709, https://doi.org/10.1007/s11999-015-4220-2.

[7] T.M. Wright, S.B. Goodman, H.C. Amstutz, National institutes of health (U.S.), American academy of orthopaedic surgeons. Implant Wear: the Future of Total Joint Replacement: Symposium, Oakbrook, Illinois, September 1995, first ed., American Academy of Orthopaedic Surgeons, Rosemont, IL, 1996.

[8] N.T. Evans, F.B. Torstrick, C.S.D. Lee, K.M. Dupont, D.L. Safranski, W.A. Chang, A. E. Macedo, A.S.P. Lin, J.M. Boothby, D.C. Whittingslow, R.A. Carson, R. E. Guldberg, K. Gall, High-strength, surface-porous polyether-ether-ketone for load-bearing orthopedic implants, Acta Biomater. 13 (2015) 159–167, https://doi.org/10.1016/j.actbio.2014.11.030.

[9] S.M. Kurtz, J.N. Devine, PEEK biomaterials in trauma, orthopedic, and spinal implants, Biomaterials 28 (2007) 4845–4869, https://doi.org/10.1016/j.biomaterials.2007.07.013.

[10] M. Mbogori, A. Vaish, R. Vaishya, A. Haleem, M. Javaid, Poly-Ether-Ether-Ketone (PEEK) in orthopaedic practice- A current concept review, Journal of Orthopaedic Reports 1 (2022) 3–7, https://doi.org/10.1016/j.jorep.2022.03.013.

[11] Z. Lyu, Y. Zhao, S. Huo, F. Wang, X. Meng, Z. Yuan, T. Long, Y. Wang, Mussel-inspired dopamine-CuII coated polyetheretherketone surface with direct and immunomodulatory effect to facilitate osteogenesis, angiogenesis, and antibacterial ability, Mater. Des. 222 (2022) 111069, https://doi.org/10.1016/j.matdes.2022.111069.

[12] A.H. Mir, M.S. Charoo, Friction and wear characteristics of polyetheretherketone (PEEK): a review, IOP Conf. Ser. Mater. Sci. Eng. 561 (2019) 012051, https://doi.org/10.1088/1757-899X/561/1/012051.

[13] Z. Cai, X. Qu, Y. Zhao, Z. Yuan, L. Zheng, T. Long, Q. Yao, B. Yue, Y. Wang, Preliminary study on immediate postoperative CT images and values of the modular polyetheretherketone based total knee arthroplasty: an observational first-in-human trial, Front. Surg. 9 (2022) 809699, https://doi.org/10.3389/fsurg.2022.809699.

[14] S.B. Goodman, Wear particles, periprosthetic osteolysis and the immune system, Biomaterials 28 (2007) 5044–5048, https://doi.org/10.1016/j.biomaterials.2007.06.035.

[15] P.A. Revell, The combined role of wear particles, macrophages and lymphocytes in the loosening of total joint prostheses, J. R. Soc. Interface 5 (2008) 1263–1278, https://doi.org/10.1098/rsif.2008.0142.

[16] C. Nich, Y. Takakubo, J. Pajarinen, M. Ainola, A. Salem, T. Sillat, A.J. Rao, M. Raska, Y. Tamaki, M. Takagi, Y.T. Konttinen, S.B. Goodman, J. Gallo, Macrophages—key cells in the response to wear debris from joint replacements, J. Biomed. Mater. Res. 101 (2013) 3033–3045, https://doi.org/10.1002/jbm.a.34599.

[17] Y. Yao, X. Cai, F. Ren, Y. Ye, F. Wang, C. Zheng, Y. Qian, M. Zhang, The macrophage-osteoclast Axis in osteoimmunity and osteo-related diseases, Front. Immunol. 12 (2021) 664871, https://doi.org/10.3389/fimmu.2021.664871.

[18] Y. Sun, J. Li, X. Xie, F. Gu, Z. Sui, K. Zhang, T. Yu, Macrophage-osteoclast associations: origin, polarization, and subgroups, Front. Immunol. 12 (2021) 778078, https://doi.org/10.3389/fimmu.2021.778078.

[19] O. Camuzard, V. Breuil, G.F. Carle, V. Pierrefite-Carle, Autophagy involvement in aseptic loosening of arthroplasty components, J. Bone Joint Surg. 101 (2019) 466–472, https://doi.org/10.2106/JBJS.18.00479.

[20] Z. Wang, N. Liu, K. Liu, G. Zhou, J. Gan, Z. Wang, T. Shi, W. He, L. Wang, T. Guo, N. Bao, R. Wang, Z. Huang, J. Chen, L. Dong, J. Zhao, J. Zhang, Autophagy mediated CoCrMo particle-induced peri-implant osteolysis by promoting osteoblast apoptosis, Autophagy 11 (2015) 2358–2369, https://doi.org/10.1080/15548627.2015.1106779.

[21] N. Liu, J. Meng, Z. Wang, G. Zhou, T. Shi, J. Zhao, Autophagy mediated TiAl 6 V 4 particle-induced peri-implant osteolysis by promoting expression of TNF-α, Biochem Bioph Res Co 473 (2016) 133–139, https://doi.org/10.1016/j.bbrc.2016.03.065.

[22] Z. Wang, Z. Deng, J. Gan, G. Zhou, T. Shi, Z. Wang, Z. Huang, H. Qian, N. Bao, T. Guo, J. Chen, J. Zhang, F. Liu, L. Dong, J. Zhao, TiAl6V4 particles promote osteoclast formation via autophagy-mediated downregulation of interferon-beta in osteocytes, Acta Biomater. 48 (2017) 489–498, https://doi.org/10.1016/j.actbio.2016.11.020.

[23] M. Ponpuak, M.A. Mandell, T. Kimura, S. Chauhan, C. Cleyrat, V. Deretic, Secretory autophagy, Curr. Opin. Cell Biol. 35 (2015) 106–116, https://doi.org/10.1016/j.ceb.2015.04.016.

[24] A. Weigert, L. Herhaus, Immune modulation through secretory autophagy, J. Cell. Biochem. (2023), https://doi.org/10.1002/jcb.30427 jcb.30427.

[25] T. Dyskova, J. Gallo, E. Kriegova, The role of the chemokine system in tissue response to prosthetic by-products leading to periprosthetic osteolysis and aseptic loosening, Front. Immunol. 8 (2005), https://doi.org/10.3389/fimmu.2017.01026.

[26] Q. Gu, Q. Shi, H. Yang, The role of TLR and chemokine in wear particle-induced aseptic loosening, J. Biomed. Biotechnol. 2012 (2012) 1–9, https://doi.org/10.1155/2012/596870.

[27] F.J. Carrión, J. Sanes, M.-D. Bermúdez, Influence of ZnO nanoparticle filler on the properties and wear resistance of polycarbonate, Wear 262 (2007) 1504–1510, https://doi.org/10.1016/j.wear.2007.01.016.

[28] P.C. Nagajyothi, S.J. Cha, I.J. Yang, T.V.M. Sreekanth, K.J. Kim, H.M. Shin, Antioxidant and anti-inflammatory activities of zinc oxide nanoparticles

synthesized using Polygala tenuifolia root extract, J. Photochem. Photobiol., B 146 (2015) 10–17, https://doi.org/10.1016/j.jphotobiol.2015.02.008.

[29] X. Meng, W. Zhang, Z. Lyu, T. Long, Y. Wang, ZnO nanoparticles attenuate polymer-wear-particle induced inflammatory osteolysis by regulating the MEK-ERK-COX-2 axis, Journal of Orthopaedic Translation 34 (2022) 1–10, https://doi.org/10.1016/j.jot.2022.04.001.

[30] M. Martínez-Carmona, Y. Gun'ko, M. Vallet-Regí, ZnO nanostructures for drug delivery and theranostic applications, Nanomaterials 8 (2018) 268, https://doi.org/10.3390/nano8040268.

[31] D.J. Klionsky, A.K. Abdel-Aziz, S. Abdelfatah, M, Guidelines for the use and interpretation of assays for monitoring autophagy (4th edition)[1], Autophagy 17 (2021) 1–382, https://doi.org/10.1080/15548627.2020.1797280.

[32] K.A. Philbrick, A.J. Branscum, C.P. Wong, R.T. Turner, U.T. Iwaniec, Leptin increases particle-induced osteolysis in female ob/ob mice, Sci. Rep. 8 (2018) 14790, https://doi.org/10.1038/s41598-018-33173-9.

[33] N. Amatya, A.V. Garg, S.L. Gaffen, IL-17 signaling: the yin and the yang, Trends Immunol. 38 (2017) 310–322, https://doi.org/10.1016/j.it.2017.01.006.

[34] R.M. Onishi, S.L. Gaffen, Interleukin-17 and its target genes: mechanisms of interleukin-17 function in disease, Immunology 129 (2010) 311–321, https://doi.org/10.1111/j.1365-2567.2009.03240.x.

[35] M. Acosta-Martinez, M.Z. Cabail, The PI3K/akt pathway in meta-inflammation, Int. J. Mol. Sci. 23 (2022) 15330, https://doi.org/10.3390/ijms232315330.

[36] R. Maitra, C.C. Clement, G.M. Crisi, N. Cobelli, L. Santambrogio, Immunogenecity of modified alkane polymers is mediated through TLR1/2 activation, PLoS One 3 (2008) e2438, https://doi.org/10.1371/journal.pone.0002438.

[37] A.P. Davies, H.G. Willert, P.A. Campbell, I.D. Learmonth, C.P. Case, An unusual lymphocytic perivascular infiltration in tissues around contemporary metal-on-metal joint replacements, J. Bone Joint Surg. 87 (2005) 18–27, https://doi.org/10.2106/JBJS.C.00949.

[38] M. Huber, G. Reinisch, P. Zenz, K. Zweymüller, F. Lintner, Postmortem study of femoral osteolysis associated with metal-on-metal articulation in total hip replacement, J. Bone Joint Surg. Am. 92 (2010) 1720–1731, https://doi.org/10.2106/JBJS.I.00695.

[39] H.-G. Willert, G.H. Buchhorn, A. Fayyazi, R. Flury, M. Windler, G. Köster, C. H. Lohmann, Metal-on-Metal bearings and hypersensitivity in patients with artificial hip joints, J. Bone Joint Surg. 87 (2005) 28–36, https://doi.org/10.2106/JBJS.A.02039pp.

[40] M. Bosetti, In vitro evaluation of the inflammatory activity of ultra-high molecular weight polyethylene, Biomaterials 24 (2003) 1419–1426, https://doi.org/10.1016/S0142-9612(02)00526-4.

[41] N. Tanabe, N. Maeno, N. Suzuki, K. Fujisaki, H. Tanaka, B. Ogiso, K. Ito, IL-1α stimulates the formation of osteoclast-like cells by increasing M-CSF and PGE2 production and decreasing OPG production by osteoblasts, Life Sci. 77 (2005) 615–626, https://doi.org/10.1016/j.lfs.2004.10.079.

[42] W. Wiktor-Jedrzejczak, A. Bartocci, A.W. Ferrante, A. Ahmed-Ansari, K.W. Sell, J. W. Pollard, E.R. Stanley, Total absence of colony-stimulating factor 1 in the macrophage-deficient osteopetrotic (op/op) mouse, Proc. Natl. Acad. Sci. U.S.A. 87 (1990) 4828–4832, https://doi.org/10.1073/pnas.87.12.4828.

[43] C.J. DeSelm, B.C. Miller, W. Zou, W.L. Beatty, E. van Meel, Y. Takahata, J. Klumperman, S.A. Tooze, S.L. Teitelbaum, H.W. Virgin, Autophagy proteins regulate the secretory component of osteoclastic bone resorption, Dev. Cell 21 (2011) 966–974, https://doi.org/10.1016/j.devcel.2011.08.016.

[44] N. Dupont, S. Jiang, M. Pilli, W. Ornatowski, D. Bhattacharya, V. Deretic, Autophagy-based unconventional secretory pathway for extracellular delivery of IL-1β, Embo J 30 (2011) 4701–4711, https://doi.org/10.1038/emboj.2011.398.

[45] T.A. Nguyen, J. Debnath, Control of unconventional secretion by the autophagy machinery, Current Opinion in Physiology 29 (2022) 100595, https://doi.org/10.1016/j.cophys.2022.100595.

[46] Y.-H. Miao, L.-P. Mao, X.-J. Cai, X.-Y. Mo, Q.-Q. Zhu, F.-T. Yang, M.-H. Wang, Zinc oxide nanoparticles reduce the chemoresistance of gastric cancer by inhibiting autophagy, World J. Gastroenterol. 27 (2021) 3851–3862, https://doi.org/10.3748/wjg.v27.i25.3851.

[47] J.P. Liuzzi, L. Guo, C. Yoo, T.S. Stewart, Zinc and autophagy, Biometals 27 (2014) 1087–1096, https://doi.org/10.1007/s10534-014-9773-0.

[48] J. Liu, Y. Kang, S. Yin, A. Chen, J. Wu, H. Liang, L. Shao, Key role of microtubule and its acetylation in a zinc oxide nanoparticle–mediated lysosome–autophagy system, Small 15 (2019) 1901073, https://doi.org/10.1002/smll.201901073.

[49] T. Kimura, J. Jia, S. Kumar, S.W. Choi, Y. Gu, M. Mudd, N. Dupont, S. Jiang, R. Peters, F. Farzam, A. Jain, K.A. Lidke, C.M. Adams, T. Johansen, V. Deretic, Dedicated SNAREs and specialized TRIM cargo receptors mediate secretory autophagy, Embo J 36 (2017) 42–60, https://doi.org/10.15252/embj.201695081.

[50] R.S. Tuan, F.Y.-I. Lee, Y.T. Konttinen, M.J. Wilkinson, R.L. Smith, What are the local and systemic biologic reactions and mediators to wear debris, and what host factors determine or modulate the biologic response to wear particles? J. Am. Acad. Orthop. Surg. 16 (2008) S42–S48, https://doi.org/10.5435/00124635-200800001-00010.

[51] S. Endres, I. Bartsch, S. Stürz, M. Kratz, A. Wilke, Polyethylene and cobalt–chromium molybdenium particles elicit a different immune response in vitro, J. Mater. Sci. Mater. Med. 19 (2008) 1209–1214, https://doi.org/10.1007/s10856-007-3104-8.

[52] X. Zhang, T. Zhang, K. Chen, H. Xu, C. Feng, D. Zhang, Wear mechanism and debris analysis of PEEK as an alternative to CoCrMo in the femoral component of total knee replacement, Friction 11 (2023) 1845–1861, https://doi.org/10.1007/s40544-022-0700-z.

[53] N.M. Lowe, W.D. Fraser, M.J. Jackson, Is there a potential therapeutic value of copper and zinc for osteoporosis? Proc. Nutr. Soc. 61 (2002) 181–185, https://doi.org/10.1079/PNS2002154.

[54] L. Popp, L. Segatori, Zinc oxide particles induce activation of the lysosome–autophagy system, ACS Omega 4 (2019) 573–581, https://doi.org/10.1021/acsomega.8b01497.